Sedimentary Geology 470 (2024) 106680

Contents lists available at ScienceDirect

Sedimentary Geology

journal homepage: www.elsevier.com/locate/sedgeo

Provenance of the late Jurassic to Cenomanian sedimentary succession of the Araripe Basin (NE Brazil) and implication for the geodynamic evolution of Western Gondwana

Mariana de Assunção Rodrigues [a,b,*], Roberto Ventura Santos [a], Martin Roddaz [b], Elton Luiz Dantas [a], Mathieu Leisen [b]

[a] Universidade de Brasília, Darcy Ribeiro Campus, Asa Norte, 70910-900 Brasília, DF, Brazil
[b] Géosciences-Environnement Toulouse, Université de Toulouse, UPS (SVT-OMP), 14 Avenue Édouard Belin, F-31400 Toulouse, France

ARTICLE INFO

Article history:
Received 24 January 2024
Received in revised form 17 May 2024
Accepted 19 May 2024
Available online 24 May 2024

Editor: Dr. Catherine Chagué

Keywords:
Provenance
Zircon U–Pb dating
Late Jurassic–Cenomanian
Araripe Basin
Western Gondwana

ABSTRACT

The separation of Gondwana was controlled by preexisting Proterozoic structures and by the development of rift aborted basins, of which the Araripe Basin (NE Brazil) is one of the best examples. Previous studies have focused on the presence and provenance of Aptian–Albian shallow-marine incursions in the Araripe Basin but to date, little attention has been given to its paleodrainage evolution during sedimentation stages. Understanding the paleodrainage evolution is crucial for determining sediment sources and how topographic changes relate to the geodynamic development of the northern part of South America during the fragmentation of Gondwana, and this study investigates the provenance of Mesozoic rift and post-rift sedimentary rocks in the Araripe Basin using a multi-proxy dataset comprising major and trace element concentrations, Sm–Nd isotopic composition, and detrital zircon U–Pb ages. The low Eu/Eu* ratios (0.3–0.9) and high Th/Sc ratios (>0.64) in the most of analyzed samples suggest a felsic and silicic source. The εNd(0) values (−12.3 to −23.7) and T_{DM} ages (1.68 to 2.55 Ga) of analyzed samples suggest overall ancient crustal sources. The presence of oval and elongated zircon grains suggests a major contribution of first-cycle transport sediments. The presence of 2.3–1.8 Ga and 0.63–0.58 Ga U–Pb zircon ages further indicates the dominant contribution of the Borborema Province influenced by the Brasiliano cycle (650–520 Ma). The low contribution of Tonian (~940 Ma) zircons to the U–Pb zircon age distribution of the rift-beginning stage sample associated with published paleocurrent direction suggests sources located in the northern and northwestern terranes of the Borborema Province. The increase of Tonian (0.9–1.0 Ga) zircon grains during the rift stage suggests a provenance change with a dominant source in the eastern terranes during the rift stage. During the post-rift I stage, the decrease of 1.2–0.72 Ga zircon ages suggests a change in the source areas, with the paleodrainage coming from northern Borborema Province, similar to that of the rift-beginning stage. The samples of the post-rift II stage exhibit dominant contributions of Paleoproterozoic and Neoproterozoic U–Pb ages related to the Albian to Cenomanian uplift of the Borborema plateau during the opening of Equatorial Atlantic Ocean. Together with previous published studies, these findings highlight the significant role played by the post-rift continental uplift to the paleodrainage of the northern part of South America.

1. Introduction

The geodynamic cycles also referred to as the Wilson Cycle (Wilson, 1969), have been responsible for the dispersal and subsequent reassembly of continents throughout Earth's history. This complex movement of continents repeats throughout geological times and has been recorded in crustal rocks since 3.0 Ga (Bleeker, 2003; Van Kranendonk et al., 2010; Shirey and Richardson, 2011). Uplift and spreading processes during the embryonic to mature stages of the ocean basins' life cycle (Wilson, 1969), the interplay between driving forces, resisting factors, and crustal weakening contribute to form a diverse range of rifts (Brune et al., 2023). The best example of these processes is the Pangea fragmentation.

The Pangea fragmentation began at the end of the Triassic and developed into three phases during the Jurassic and Cretaceous (Moulin et al., 2010; Heine et al., 2013). Three superblocks were formed after an Early Jurassic disruption driven by geodynamics, kinematic, and plate tectonic changes in Western Gondwana (Matos, 1999; Sahabi et al., 2004; Eagles

* Corresponding author at: Universidade de Brasília, Darcy Ribeiro Campus, Asa Norte, 70910-900 Brasília, DF, Brazil.
E-mail addresses: mariana.rodrigues@get.omp.eu (M.A. Rodrigues), rventura@unb.br (R.V. Santos), martin.roddaz@get.omp.eu (M. Roddaz), elton@unb.br (E.L. Dantas), mathieu.leisen@get.omp.eu (M. Leisen).

https://doi.org/10.1016/j.sedgeo.2024.106680

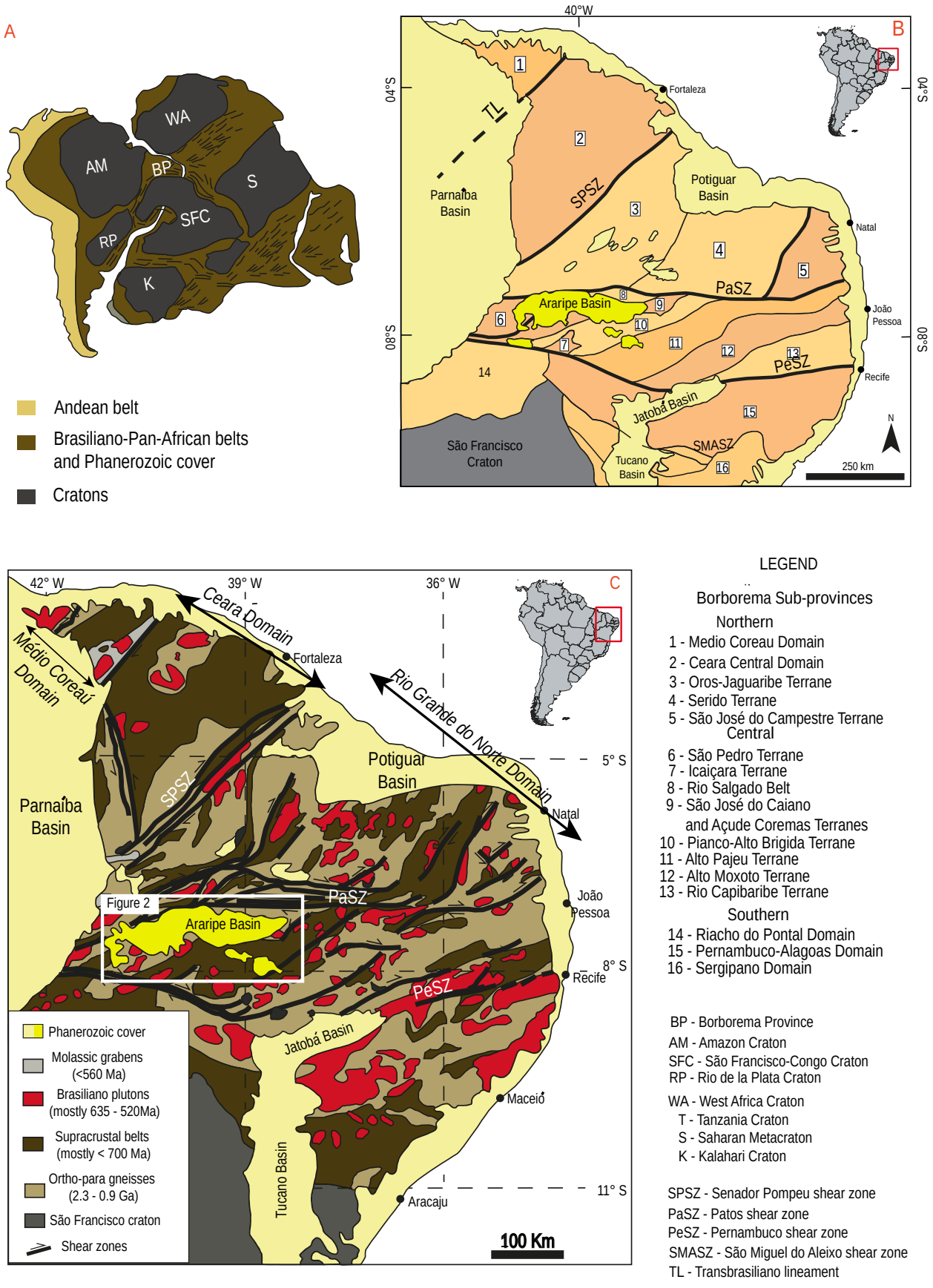

Fig. 1. Pre-drift reconstruction of South America and Africa showing the Andean belt, Archean/Proterozoic cratons, and Brasiliano/Pan-African provinces of western Gondwana. (B) Tectonic compartmentation of Borborema Province with the division into Northern, Central, and Southern sub provinces. (C) The schematic map of the Borborema Province shows the Northern and Southern sub-province subdivisions. Map based on Ferreira et al. (1998), Van Schumus et al. (2011), Neves et al. (2015), de Brito Neves and Campos Neto (2016) de Brito Neves and Passarelli (2020), Matos et al. (2021a, 2021b), and Godot Souza et al. (2022).

and König, 2008; Moulin et al., 2010; Heine et al., 2013). Before the Cretaceous breakup, an early rift basin developed in the central and northern Gondwana within the so-called Afro-Brazilian Depression (Assine, 2007; Kuchle et al., 2011; Scherer et al., 2014; Guzmán-González et al., 2020). The rifting between South America and Africa was diachronic and controlled by preexisting Proterozoic structures (Matos, 1992). In the Borborema Province (Northeast Brazil, Fig. 1), the Mesozoic sedimentary record of the rift basins (i.e. Araripe, Rio dos Peixes, Potiguar) provides important constraints on the geodynamic and tectonic processes that controlled the dislocation of Western Gondwana. However, the evolution of these rift basins was aborted during the opening of the South and Equatorial Atlantic Oceans, which occurred between 90 and 135 Ma (Heine et al., 2013; Hall et al., 2018; Dummann et al., 2023). The Araripe Basin is an example of an aborted rift basin that formed along the Cariri-Potiguar trend (Matos, 1992; Camacho and Sousa, 2017) (Fig. 1). This basin is located on the Precambrian terranes of the Transverse Zone in the Borborema Province (Assine, 2007; Fambrini et al., 2020; de Brito Neves et al., 2023) (Fig. 1) and has a unique record of pre-rift to post-rift sediments.

Deciphering the long-term evolution of paleodrainages is important to understand how topographic changes are related to the geodynamic evolution of large continental areas, such as the northern part of South America during the Gondwana fragmentation. To depict the paleodrainage evolution, provenance studies are important. The provenance of the meso-Cenozoic sedimentary record of the Amazonian basins was addressed by different studies (Basu et al., 1990; Roddaz et al., 2005, 2012, 2021; Figueiredo et al., 2009; Hoorn et al., 2017; van Soelen et al., 2017; Horbe et al., 2019; Rodrigues et al., 2023). In contrast, little is known about the provenance of the Mesozoic sedimentary succession of the Araripe Basin. Most of the paleogeographic studies focused on the existence and provenance of the Aptian–Albian shallow marine incursions that have affected the Araripe Basin (Machado Junior et al., 1990; Assine, 1994; Arai, 2014, 2016; Custódio et al., 2017; Godot Souza et al., 2022). To date, no study has addressed the paleodrainage scenario during the rift stage and post-rift stage, after the continental break-up.

In this study, we present new whole-rock and zircon geochemistry, Sm–Nd isotopic composition, and U–Pb detrital zircon ages to characterize the sedimentary provenance during the tectonic stages of the Araripe Basin based on the academic thesis by Rodrigues (2023). Our data extend and complement the first U–Pb zircon dataset published by Godot Souza et al. (2022) and will help to better understand and reconstruct the evolution of the Araripe Basin during the rift and post-rift stages.

2. Geological setting

2.1. Borborema Province

The Borborema Province (Almeida et al., 1981) is located in the northeastern South American Platform and represents a mosaic of tectonic blocks with Paleoproterozoic basement and scattered Archean nuclei, Meso to Neoproterozoic supracrustal rocks, and large intrusions of granitic rocks emplaced during the Neoproterozoic Brasiliano orogen, from 650 to 520 Ma (de Brito Neves et al., 2000; van Schmus et al., 2008, 2011; da Cruz et al., 2014) (Fig. 1). This complex orogenic system resulted from the breakup of a Paleoproterozoic supercontinent during the late Mesoproterozoic to early Neoproterozoic (van Schmus et al., 2008; Guimarães et al., 2016). The Borborema Province is situated between the West Africa–São Luis craton to the north, the late Neoproterozoic terranes (Brasiliano/Pan African), and the Phanerozoic Parnaíba Basin to the west. It is limited to the south by the São Francisco–Congo Craton (Fig. 1) (Pimentel and Fuck, 1992; de Brito Neves et al., 2000; Guimarães et al., 2016). It is possible to identify structural and tectonic continuations of the Borborema Province in the African continent, mainly in the domains of the Trans-Saharan and Central Africa Orogens (Caxito et al., 2020).

Three major sub-provinces were proposed to divide the Borborema Province: the northern, central, and southern sub-provinces (de Brito Neves et al., 2000; Neves, 2003; Van Schmus et al., 2008, 2011; Santos et al., 2010; Neves et al., 2015) (Fig. 1). The Northern subprovince, located north of the Patos Shear Zone System (PaSZ) includes the Rio Grande do Norte, Ceará, and Médio Coreaú domains (Fig. 1) and consists of various geological groups from the Archean (São José do Campestre Massif and Granjeiro Complex (Dantas et al., 2004; Dantas et al., 2013; Freimann, 2014; Vieira, 2019; Archanjo et al., 2021)), and Paleo- to Neoproterozoic supracrustal rocks, and granitic intrusions (de Brito Neves et al., 2000, 2003; Van Schmus et al., 2003; Archanjo et al., 2021).

The Central subprovince, known as the Transversal Zone Domain (de Brito Neves et al., 2000), lies between the Patos and Pernambuco shear zone systems (PeSZ). It is characterized by transcurrent faults such as the "Paraíba transversal zone" and "Pernambuco transversal zone" (Ebert, 1970; Van Schmus et al., 2011) (Fig. 1). This zone experienced block rotation during the late Brasiliano fragmentation (Jardim Sá et al., 1992; Van Schmus et al., 2011), hosting several defined terranes based on structure, geology, and geochronology (Santos et al., 1998; de Brito Neves et al., 2000; Van Schmus et al., 2011) (Fig. 1, Table 1). The Açude Coremas, São José do Caiana, and Icaiçara Terranes, located on the western side of the Transversal Zone Domain, share lithological and structural similarities and possess pre-Brasiliano basement inliers of Paleoproterozoic ages (de Brito Neves and Passarelli, 2020). The Piancó-Alto Brígida Terrane in the eastern part consists of late Neoproterozoic rocks (Cariris Velhos suite and Santana do Garrotes Formation (1000–640 Ma)) formed during the Cariris Velhos event (de Brito Neves et al., 2005; Santos et al., 2010; Van Schmus et al., 2011).

The Pernambuco shear zone system (PeZS) separates the Central and Southern subprovinces. The latter encompasses the Sergipano and Riacho do Pontal belts and the Pernambuco–Alagoas Domain, which can be divided into Western and Eastern segments, separated by the Tucano–Jatobá Cretaceous sedimentary basin (Angelim and Kosin, 2001; da Cruz et al., 2014; Neves et al., 2015) (Fig. 1). The Riacho do Pontal Belt has Archean basement lenses (2.7–3.0 Ga), late Neoproterozoic plutons (920–1000 Ma), and Neoproterozoic metavolcanosedimentary units (de Brito Neves et al., 2015). The western segment of the Pernambuco–Alagoas Domain is formed by the Mesoproterozoic paragneiss complex which presents several detrital zircon populations with Neoarchean (2.6–2.7 Ga), Paleoproterozoic (1.9–2.0 Ga) and Stenian–Tonian (875–1050 Ma) U–Pb ages (da Cruz et al., 2014).

2.2. Intracontinental basins

2.2.1. Parnaíba Basin

In the northeast part of the South America Platform, the Phanerozoic Parnaíba Basin represents a cratonic basin, formed during the post-collisional stages of the Brasiliano Pan-Africano event (Vaz et al., 2007; Assis et al., 2019). The sedimentation occurred during the Gondwana amalgamation in the Ordovician (De Castro et al., 2014; Assis et al., 2019). Three large transgressive–regressive depositional sequences were identified: the Silurian Serra Grande, the Devonian Canindé, and the Permo-Triassic Balsas Group (Góes and Feijó, 1994; Góes, 1995; Vaz et al., 2007; Hollanda et al., 2014) highlighting two other depositional sequences: the Jurassic Pastos Bons Formation and the Cretaceous Corda, Grajaú, Codó, and Itapecuru formations. Detrital U–Pb zircon ages from the first three sequences indicate contributions from Rhyacian–Orosirian (2.3–2.05 Ga), Stenian–Tonian (1.2–0.72 Ga), and Ediacaran (635–541 Ma) sources, probably originated from the southern and central parts of the Borborema Province (Hollanda et al., 2014). During the Triassic–Jurassic (Mosquito Formation) and Cretaceous (Sardinha Formation), several magmatic events affected the Parnaíba Basin (Heilbron et al., 2018; Klöcking et al., 2018; Miloski et al., 2019). Basaltic dykes, sills, and other mafic magmatic bodies occurred interlayered with and intruded in thick sedimentary succession (Miloski et al., 2019).

2.2.2. Araripe Basin

The Araripe Basin is >9000 km^2 and is one of the largest basins located in northeast Brazil. It was formed during the break-up of

Table 1
Borborema Province sub-division with general information about rock types, U–Pb ages, and Sm–Nd isotopic compositions.

Borborema Province					
Domain/terrane	Type of rocks	Age (Ga)	εNd (0)	T_{DM} (Ga)	References
Northern sub-province					
Médio Coreaú Domain	Orthogneiss, migmatites (Granja Complex); paragneiss (Martinopole Group); volcano-sedimentary rocks; granitoids	2.35–2.27 (Granja Complex) 0.77 (Martinopole Group) 0.56–0.52 (granitoids)		2.38–2.61	Santos et al. (2008), Fetter et al. (2000), Araujo et al. (2012)
Ceará Central Domain	Granitoids (Tamboril–Santa Suiteria Complex); metasedimentary rocks (Ceará Group)	0.65–0.61 (granitoids)	−21.48 to −19.09 (granitoids)	2.19–2.69 (granitoids)	Costa et al. (2013)
		1.8–0.74 (detrital zircon)	−25.79 to +2.12 (metasediments)	1.95–2.4 (metasediments)	Arthaud et al. (2015)
Orós-Jaguaribe Terrane	Metasedimentary and metavolcanic rocks; orthogneiss	1.9–0.65	–	–	Parente and Arthaud (1995), Arthaud et al. (2008)
Seridó Terrane	Orthogneiss; metasupracrustal rocks	2.4–1.74	−37.51 to −28.69	3.20–2.5	Hollanda et al. (2011)
São José do Campestre Terrane	Granitoids and metasupracrustal rocks	3.45–2.70	−6.18 to +3.36	4.1–3.2	Dantas et al. (2013), Dantas et al. (2004)
Central sub-province					
São Pedro Terrane	Orthogneisses (TTG, granites, granodiorite) "Granjeiro Complex"	3.3–2.5	−22.64 to −43.78	2.29 to 3.48	Archanjo et al. (2021)
	Metavulcano-sedimentary rocks (Ipueirinha Group)	Archean and Neoproterozoic	−5.2 to −27.3	1.13 to 3.16	Brito Neves et al. (2022)
	Orthogneisses; granites and supracrustal rocks (metamorphic rocks) "Ouricuri and Bodocó"	2.0–2.3	−6.67 to −29	1.3 to 2.4	
Açude Coremas Terrane	Orthogneisses; granites ("Itaporanga"); Brasiliano granites	2.0–2.1	−6.3 to −28.38	1.17 to 2.92	de Brito Neves and Passarelli (2020)
	Metamudstones (Unidade Bom Jesus)	0.61			
São José do Caiana	Orthogneisses; paragneisses granites; Brasiliano granites; metasedimentary rocks	2.1–2.2	−14.98 to −29.38	1.8 to 2.7	de Brito Neves and Passarelli (2020), Kozuch (2003), Scherer et al. (2014)
Icaiçara Terrane	Ortho-paragneisses "Complexo Parnamirim" and "Barro Complex"; migmatites; metasedimentary rocks	2.0–2.1 0.99–0.95	−8.95 to −28.46	1.3 to 2.3	de Brito Neves and Passarelli (2020)
Piancó-Alto Brígida Terrane	Metasedimentary, metavolcanic, and metaplutonic rocks; granitoids	1.0–0.64	−43.6 to −2.0	1.08–2.5	de Brito Neves et al. (2005), Van Schmus et al. (2011)
Alto Pajeú Terrrane	Ortho and paragneiss; mylonite; granitoids; metasedimentary, metavolcanic, and metaplutonic rocks	2.1 to 0.64	−32.8 to −6.4	1.04–3.09	Rodrigues and de Brito Neves (2008); Santos et al. (2010); de Brito Neves et al. (2005); Van Schmus et al. (2011)
Alto Moxotó Terrane	Ortho and paragneiss (Sertânia Complex); amphibolite; granites	2.1–2.3 (orthogneiss) 2.2–1.9 (detrital zircons)	−25.0 to −16.7	2.2–2.5	Santos et al. (2004); Rodrigues and de Brito Neves (2008); de Brito Neves et al. (2001); de Brito Neves et al. (2005); Van Schmus et al. (2011)
Rio Capibaribe Terrane	Metasedimentary rocks; orthogneiss; tonalites		−23.2 to −5.3	2.2–1.3	de Brito Neves et al. (2005); Van Schmus et al. (2011)
Southern sub-province					
Riacho do Pontal Domain	Granites; schist; gneiss	3.0–0.92	−15.1 to −7.9	1.43–1.60	de Brito Neves et al. (2015); Van Schmus et al. (2011)
Pernambuco–Alagoas Domain	Ortho and paragneiss; granitoids	2.6–0.87	−38.3 to −8.00	1.37–3.59	da Cruz et al. (2014)
Sergipano Domain	Metasedimentary and metavolcanic rocks; granitoids; orthogneiss and migmatites	2.83 (orthogneiss) Neoproterozoic plutons	–	–	D'el Rey Silva (1995); Silva Filho and Torres (2002)

Gondwana and the opening of the South Atlantic Ocean (Assine, 1992, 2007; Matos, 1992; Maisey, 2000; Fambrini et al., 2020). The Araripe Basin comprises five sequences and represents a rift aborted sedimentary basin which starts during the Jurassic and ends in the Early Cretaceous.

The Cariri Formation (Beurlen, 1962) outcrops on the eastern side of the Araripe Basin and it is formed by fluvial coarse-grained sandstones and conglomerates (Assine, 1992, 2007; Silvestre et al., 2017; Fambrini et al., 2020). The age of this formation is under dispute (Caputo and Crowell, 1985; Assine, 1992, 2007; Coimbra et al., 2002; Fambrini et al., 2020), but a recent study suggests an Ordovician age (Cerri et al., 2022). The Cariri Formation is sourced from Neoproterozoic, Cambrian, and Paleoproterozoic rocks from the Transversal and Southern zones of the Borborema Province (Cerri et al., 2022), and represents the pre-rift sequence.

The mudstones of the Brejo Santo Formation were deposited during the late Jurassic extensional events that affected the northern Gondwana and the pre-rift sequence (Garcia and Wilbert, 1995; Ponte and Ponte Filho, 1996; Assine, 2007; Fambrini et al., 2013, 2020; Vieira Melo and Carvalho, 2018) followed by the deposits of the Tithonian Missão Velha Formation corresponding to the "Rift-beginning stage". The Missão Velha Formation consists of fluvial sandstones with paleocurrents toward SE and presents fossil wood fragments (*Dadoxilon benders* (Brito, 1987)) (Assine, 2007; Scherer et al., 2014; Fambrini et al., 2020).

The Neocomian Abaiara Formation is related to the implantation of half-graben systems in the Araripe Basin during the Rift stage (Assine, 2007; Scherer et al., 2014; Fambrini et al., 2020). It comprises the fluvio-deltaic–lacustrine deposits with dispersed paleocurrents (Scherer et al., 2014). The presence of syn-depositional normal faults indicates active extensional tectonics during the sedimentation (Scherer et al., 2014). However, the rift sedimentation was aborted when the major deformation started at the Equatorial branch (Matos, 1992). Erosive processes predominated until the Aptian, causing erosion of the high blocks and peneplanation of the relief (Assine, 2007).

The post-rift deposition of the Araripe Basin is divided in two sequences. The fluvial, lacustrine, and transitional marine Aptian–Albian Santana Group ("Post-rift I") is formed by the Barbalha, Crato, Ipubi, and Romualdo formations (Neumann et al., 2003; Assine, 2007). The basal Barbalha Formation is characterized by fining upward sandstone with mudstone interval sequences (Assine, 1992) with a black shale interval with limestones termed the Fundão Member (Rios Netto et al., 2012a), or Batateiras layer (Hashimoto et al., 1987; Assine et al., 2014). Palynological analyses in the black shale layer indicate late Aptian ages (Lima and Perinotto, 1984; Hashimoto et al., 1987; Barbosa et al., 2006; Rios Netto et al., 2012b). The basal fluvial paleocurrents measured by Assine (1994) present SE direction. The Crato Formation is characterized by micritic laminated limestones interlayered with calciferous shales (Assine, 2007; Fambrini et al., 2020). The rich fossiliferous association suggests a lacustrine paleoenvironment (Assine et al., 2014) during the late Aptian (Lima, 1978; Assine, 2007). Evaporitic sedimentary rocks of the Ipubi Formation succeeded the sedimentary rocks of the Crato Formation (Assine et al., 2014). The fossiliferous-rich conglomerates, fine-coarse sandstones, shales, and limestones of the Romualdo Formation were deposited in a shallow marine environment (Assine et al., 2014; Custódio et al., 2017). Paleocurrents measured in tidal-influenced sandstones indicate NNW–SSE paleocurrent directions (Custódio et al., 2017). The age of the Romualdo Formation is early to middle Aptian or early Albian and based on microfossils (Coimbra et al., 2002; Heimhofer and Hochuli, 2010), whereas, palynological data indicate a late Aptian age (Rios Netto et al., 2012b).

The Post-rift II sequence starts with the Araripina Formation, which overlays the Romualdo Formation in the eastern part of the basin and rests directly on the basement in the western part (Assine, 2007; Fambrini et al., 2020). It is formed by fine to coarse-grained sandstones deposited in a lagoon paleoenvironment (Assine, 2007). Palynological associations suggest a mid-Albian age (Lima, 1978). The Albian–Cenomanian Exu Formation is characterized by fluvial sandstones (Assine, 2007) with paleo flows to the west interpreted to have come from the eastern Borborema Province (Assine, 2007).

3. Methods

3.1. Sampling and stratigraphic constraints

In total, we collected thirty-nine samples from the Cretaceous sedimentary rock successions cropping out in the Araripe Basin (Fig. 3 and details in the Supplementary dataset). Eleven samples were analyzed for zircon U–Pb dating and zircon trace elements. To improve the statistical quality of our interpretations, we used the U–Pb zircon ages published by Godot Souza et al. (2022) (Figs. 2, 3; Table S1 in the Supplementary dataset). Nineteen samples were measured for their bulk major and trace element concentrations, and nine for their Sm–Nd isotopic composition. The locations of the analyzed samples can be found in Fig. 2 and Table S1 in the Supplementary dataset.

Two samples (M2AR 4-2; M2AR 4-1) were collected in sandstone and siltstone levels of the Rift-beginning sequence of the Brejo Santo Formation, exposed along the Transnordestina railway, near Brejo Santo city (Fig. 2, Table S1 in the Supplementary dataset). M2AR 4-2 was collected for major and trace element concentrations and Sm–Nd isotope analyses, and M2AR 4-1 was collected for U–Pb age analyses. M2AR 5-1 and M2AR 3-1 samples were collected in the Rift stage sequence. Both samples were used for U–Pb zircon analyses in the Abaiara Formation outcrop exposed in the BR-116 highway, near the Padre Cícero Village in the Milagres city (Fig. 2, Table S1 in the Supplementary dataset).

Three samples were collected from the "Post-rift I" Barbalha Formation. The M2AR 8-1 sample was collected in the fluvial facies of the lower Barbalha Formation at the Salamanca River valley described by Scherer et al. (2015) and Fambrini et al. (2016, 2019), and was analyzed for U–Pb zircon ages. M2AR 9-1 was collected in the Rio da Batateira Geosite, the eastern sector of the Crato city (Figs. 2, 3 and Table S1 in the Supplementary dataset) and corresponds to the Batateira Layer (Assine, 2007) or Batateira Formation (Ponte and Appi, 1990). This sample was analyzed for major and trace element concentrations and Sm–Nd isotope analyses. Godot Souza et al. (2022) analyzed the ARA-05 sample from the same sedimentary succession for U–Pb age. M2AR 11.1 was collected in the upper part of the Barbalha Formation in the Chico da Cascata passage above the Batateira Layer (Assine, 2007) and was analyzed for U–Pb zircon ages.

The M2AR 10I and 10.75II samples were collected in the outcrop exposed at the Três Irmãos Mine and were analyzed for U–Pb zircon ages and major and trace element concentrations. Godot Souza et al. (2022) collected the ARAP-47 sample in the same outcrop (Fig. 3). M2AR 10I was collected in the laminated sandstones, and M2AR 10.75 II in the gray-colored shale level (see Fig. 5 in Godot Souza et al. (2022)). Three outcrops of the "Post-rift I" Romualdo Formation were sampled. The M2AR 2-2 and M2AR2-3 samples were collected on the western side of the basin near Araripina city (Fig. 2), in the thin layers of coquinas and limestone coquinoids (Sales, 2005; Prado et al., 2015; Fambrini et al., 2020). These samples were analyzed for their major and trace element concentrations. On the eastern side of the basin, we collected seventeen samples from the Mãozinha and Sobradinho outcrops (Fig. 2, Table S1, and Fig. S1 in the Supplementary dataset), which were described in Custódio et al. (2017). At the Sobradinho outcrop, we collected two samples for U–Pb zircon analyses (M2AR 7-2; 7-5), and nine samples (M2AR 7-3; 7-4; 7-5BS; 7-6; 7-7; 7-8 XI; 7-8XII; 7-8 VII; 7-8 VIII BS) for major and trace element concentrations and Sm–Nd isotopic composition. At the Mãozinha outcrop, we collected two samples for U–Pb zircon analyses (M2AR 6-1; 6-9D), and four samples (M2AR 6-2; 6-3; 6-9BS; 6-8BS) for major and trace element concentrations and Sm–Nd isotopic composition (Fig. 3).

The "Post-rift II" sequence Araripina Formation and Exu Formation outcrops are exposed along the PI-142 road between Marcolândia and Caldeirão Grande cities on the crystalline basement (Fig. 2 and Fig. S1 in the Supplementary dataset). We collected two samples from the Araripina Formation: a coarse-grained sandstone (M2AR 1-3) for U–Pb zircon ages, and siltstone (M2AR 1-3) for major and trace element concentrations and Sm–Nd isotopic isotopes. The M2AR 1-4 and M2AR 1-5 samples were collected in the Exu Formation for major and trace element concentrations, Sm–Nd isotopic composition, and U–Pb zircon analyses.

3.2. Major and trace element concentrations

The major and trace element concentrations and loss on ignition (LOI) were measured at the Service d'Analyse des Roches et Mineraux (SARM, INSU facility, Vandoeuvre-Les-Nancy, France) by ICP-OES and ICP-MS. Analytical details are available at https://sarm.cnrs.fr/index.html/ and in Carignan et al. (2001). Precision is better than 5 % for elements measured by ICP-OES, and 10 % for elements measured by ICP-MS (see Supplementary dataset for details). The major elemental concentrations (LILE, HFSE, and TTE) of the analyzed samples were normalized to the Post Archean Australian Shales (PAAS) concentrations (Taylor and McClennan, 1985; Pourmand et al., 2012). We used the major element concentrations to calculate the chemical index of alteration (CIA). It is defined as $CIA = [Al_2O_3 / ((Al_2O_3 + CaO^* + Na_2) + K_2O)] \times 100$ (in molar proportions), in which CaO^* represents the CaO content in the silicate fraction (Nesbitt and Young, 1982).

3.3. Sm–Nd isotope composition

The samples were processed for Sm–Nd isotopes at the Geochronos Laboratory of the Geosciences Institute of the Universidade de Brasília. Before chemical preparation, the samples were dried at 60 °C for approximately 12 h. Sample digestion and extraction of Sm–Nd isotopes follow the procedures described in Goia and Pimentel (2000). The isotopic ratios of both elements were measured using a Thermo Scientific TRITON Plus thermal ionization mass spectrometer. During

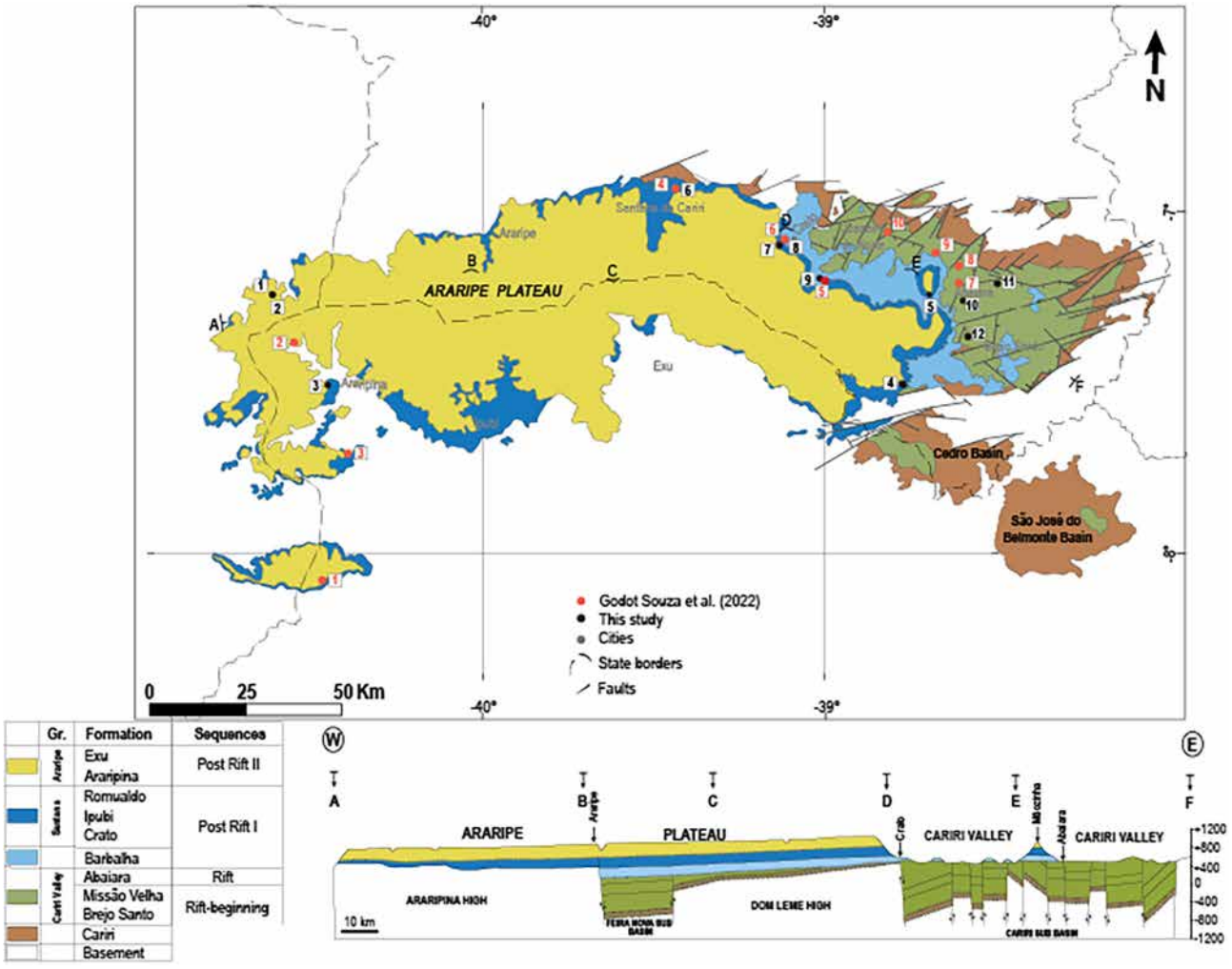

Fig. 2. Geological map of the Araripe Basin showing the stratigraphic record of the rift-beginning, rift, and post-rift stages (modified from Assine, 2007 and Fambrini et al., 2020). The number in the map refers to samples from this study (black) and Godot Souza et al. (2022) (red).

the Nd runs, isotopic normalizations were made using the natural ratios of $^{146}Nd/^{144}Nd = 0.7219$. The accuracy of the measurements was estimated by repeated analysis of the BHVO-2 standard. Repeated analysis of the BHVO-2 standard gave a $^{143}Nd/^{144}Nd$ ratio of 0.512996 ± 0.000006 (2SD, n = 10) (Weis et al., 2005).

The measured $^{143}Nd/^{144}Nd_{sample}$ and $^{143}Sm/^{144}Nd_{sample}$ ratios were expressed in epsilon notation and reflect the fractional deviation in parts per 10^4 unit from the $^{143}Sm/^{144}Nd$ from the Chondritic Uniform Reservoir (CHUR). This notation is defined as:

$$_{\varepsilon}Nd\ (t) = \left[\left(^{143}Nd/^{144}Nd\right)_{sample}\ (t)/\left(^{143}Nd/^{144}Nd\right)_{CHUR}\ (t) - 1\right] \times 10^4$$

where t indicates the time at which $_{\varepsilon}Nd$ is calculated. Here, no time correction was applied (t = 0), and the $^{143}Nd/^{144}Nd_{CHUR}\ (0) = 0.512638$ (Jacobsen and Wasserburg, 1980).

The TDM and TDM* ages were calculated as follows (DePaolo, 1981; DePaolo et al., 1991; Augustsson and Bahlburg, 2008).

$$T_{DM} = \ln\left[\left(^{143}Nd/^{144}Nd_{sample,today} - ^{143}Nd/^{144}Nd\right)_{DM,today}\right)/\left(^{147}Sm/^{144}Nd_{sample,today} - ^{147}Sm/^{144}Nd_{DM,today}\right) + 1]/\lambda;$$

$$T_{DM^*} = \ln[\left(^{143}Nd/^{144}Nd_{sample,Ts} - ^{143}Nd/^{144}Nd\right)_{DM,Ts})/\left(^{147}Sm/^{144}Nd_{crust,Ts} - ^{147}Sm/^{144}Nd_{DM,Ts}\right) + 1]/\lambda + Ts;$$

where Ts is the estimated stratigraphic age. For the $^{147}Sm/^{144}Nd_{crust}$, Ts was calculated assuming that the $^{147}Sm/^{144}Nd_{crust,\ today} = 0.11$ (Albarède and Brouxel, 1987). The model of Goldstein et al. (1984) was used, where $\lambda\ (^{147}Sm) = 6.54 \times 10^{-12}\ a^{-1}$, $^{143}Nd/^{144}Nd_{DM,\ today} = 0.51315$, $^{147}Sm/^{144}Nd_{DM,\ today} = 0.217$, $^{143}Nd/^{144}Nd_{CHUR} = 0.512638$, and $^{147}Sm/^{144}Nd_{CHUR,\ today} = 0.1967$.

3.4. Detrital zircon

3.4.1. U–Pb geochronology and trace element concentrations

The samples were processed at the Geochronos Laboratory of the Geosciences Institute of the University of Brasília (Brazil). First, they were fragmented in a rock crusher, sifted, and concentrated using a pan to separate the heavy mineral fraction. A Frantz magnetic separator was used to remove the magnetic fraction. At the Géosciences Environnement Toulouse (GET) (France) laboratory, approximately 150 zircons were handpicked from each sample under a binocular microscope and mounted in epoxy resin. The resin disks were then polished, cleaned, and carbon-coated, then, cathodoluminescence (CL) images of zircon grains were obtained using a scanning electron microscope (SEM) Tescan Vega 4 equipped with a Bruker 30mm^2 EDS system, working at 10 kV with a beam current of 3 10 nA.

Trace element concentrations and U–Pb ages in zircons were measured with an Element HR-ICPMS (ThermoScientific) coupled with a femtosecond laser (ESI — New Wave NWRfemto) at the ICPMS laboratory of Géosciences Environnement Toulouse GET, Toulouse, France. Before each analysis session, the ICP-MS was tuned by ablating a NIST SRM 610 glass reference material (Jochum et al., 2011), to ensure acceptable levels of sensitivity, stability, oxide, and fractionation (U/Th).

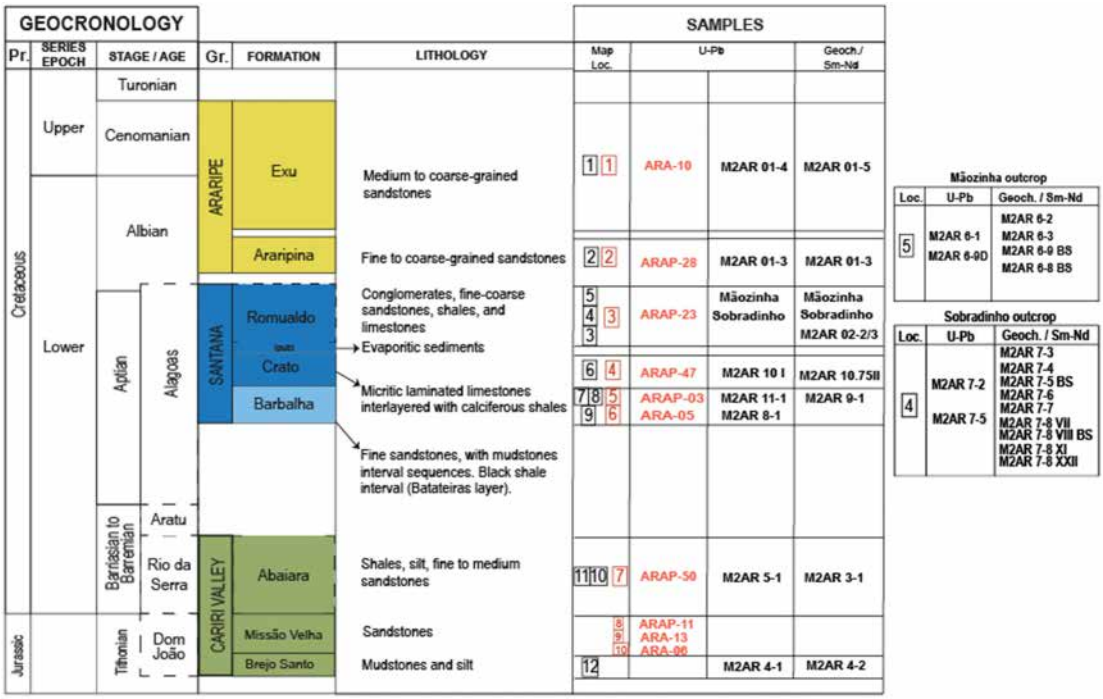

Fig. 3. Stratigraphic chart of the Araripe Basin (taken from Assine, 2007) showing the samples analyzed in this study (in black color) and by Godot Souza et al. (2022) (in red). Loc. and Geoch. refer to location and major and trace element analysis respectively. The lithology description was based in Assine (2007) and Fambrini et al. (2020).

The analytical conditions of the LA-ICPMS system were: spot size of 30 μm, frequency of 8 Hz, and fluence of ~2 J/cm^2. The GJ-1 (Jackson et al., 2004) was used as the primary standard, and Nist SRM (Jochum et al., 2011) for trace element analysis. Si (stoichiometric content 15.38 %) was employed as an internal standard to determine trace element concentration in the zircons. The accuracy and reproducibility of the analyses were checked by repeated analyses of reference materials (91500 (Wiedenbeck et al., 2004); Plesovice (Sláma et al., 2008); AUS-7 (Kennedy et al., 2014); Maniitsoq (Marsh et al., 2019)) (see Supplementary dataset for details). Data processing and correction of laser-induced fractionation (LIEF) were performed using the IOLITE v4.0 software (Paton et al., 2011) as a time-resolved signal, and individual signal inspection was done with the assistance of VisualAge (Petrus and Kamber, 2012) with exponential plus linear modeling. Our measurements of 91500 yielded weighted mean $^{206}Pb/^{238}U$ ages of 1063 ± 10 Ma (2σ, n = 309) in agreement with the recommended age of 1062.4 ± 0.4 Ma (Wiedenbeck et al., 1995).

The effective U–Pb ages were $^{206}Pb/^{238}U$ ages for zircon grains with ages ≤1.5 Ga and $^{207}Pb/^{206}Pb$ ages for grains with ages >1.5 Ga (Spencer et al., 2016). Ages with discordance degrees >10 % and samples with few zircons were not considered because of their low statistical representation (Vermeesch, 2004). Detrital zircon age data are visualized and compared using kernel density estimation (KDE) diagrams (Vermeesch, 2013). To investigate the difference between detrital zircon U–Pb age distributions, we implemented the non-matrix metric multi-dimensional scaling (MDS) statistical technique (Vermeesch, 2013). The MDS is a "superset of principal component analysis" that, given a table of pairwise 'dissimilarities' between samples, produces a 'map' of points on which 'similar' samples cluster closely together, and 'dissimilar' samples plot far apart (Vermeesch, 2018). Following the latest recommendations by Vermeesch (2018), we use the Kolmogorov–Smirnov test to produce an MDS map comparing analyzed samples.

3.4.2. Morphology

For the morphology characterization of analyzed zircons, we adopted the roundness and elongation classifications proposed by Augustsson et al. (2018). These classifications are specifically applicable to grains with concordant U–Pb ages. Broken grains without obvious detrital shapes in the CL images were not analyzed. Regarding roundness, we employed a simplified version of Powers's (1953) and Gärtner et al.'s (2013) framework, categorizing grains as euhedral, subangular to subrounded, or rounded. For elongation, we relied on length-to-width ratios to differentiate between round crystals (with ratios below 1.3), oval crystals (ranging from 1.3 to 1.8), and elongated crystals (exceeding 1.8) (Powers, 1953).

4. Results

4.1. Major elements, large-ion lithophile elements (LILE), high field strength elements (HFSE), and trace transition elements (TTE)

On the eastern part of the Araripe Basin, the rift-beginning sample M2AR 4.2 (Brejo Santo Formation) is strongly depleted in MgO, Na_2O, K_2O, Sc, Rb, Cs, Ba, and Sr relative to PAAS. The post-rift I M2AR 9.1 (Barbalha Formation) sample is strongly enriched in MnO, CaO, P_2O5, Y, Nb, V, Co, Cu, and Ni relative to PAAS. The M2AR 10.75 II sample (Crato Formation) has enrichment in MnO, MgO, CaO, Sr, Y, and Nb. All the post-rift I samples from the Sobradinho outcrop (Romualdo Formation) are depleted in Al_2O_3, Na_2O, TiO_2, Cs, K_2O (except for M2AR 7.6), P_2O_5, Sc (except for M2AR 7.6 and 7.8 VIII), SiO_2 (except for M2AR 7.4) and Ba (excepted M2AR 7.8 VII) against PAAS. High enrichment in CaO is noted for M2AR 7.8 XI, M2AR 7.7, M2AR 7.5, M2AR 7.8 VII, and M2AR 7.8 XXII samples, while all other samples from the Sobradinho outcrop are depleted against PAAS (Table S7 in the Supplementary data). All the post-rift I samples from the Mãozinha outcrop (Romualdo Formation) (M2AR 6.9, M2AR 6.8, M2AR 6.3, M2AR 6.2) are depleted in Al_2O_3, Na_2O, TiO_2, Cs, Sr, and V against PAAS and all the samples present slight enrichment in K_2O and high enrichment in MgO and Nd against the PAAS (Table S7 in the Supplementary data and Fig. 5). On the western part of the Araripe Basin, the post-rift I stage samples M2AR 2.3 and M2AR 2.2 (Romualdo Formation) are enriched in CaO and MnO against the PAAS. M2AR 2.3 is also enriched in P_2O_5. All other elements are depleted relative to PAAS. Post-rift II M2AR 1.3 (Araripina Formation) is depleted in SiO_2, Fe_2O_3, MgO, Rb,

Cs, Ba, Sr, Y, Nb, V, Co, Cu, and Ni relative to PAAS. The M2AR 1.5 sample (Exu Formation) is enriched in SiO_2, TiO, P_2O_5, Sr, Zr, Nb, Hf, and Cr relative to PAAS (Table S7 in the Supplementary data and Fig. 5).

The CIA can be useful for indicating the degree of source-area weathering and the paleo-weathering conditions of ancient sediments (Nesbitt and Young, 1982; Fedo et al., 1995). We do not have CO_2 data for our analyses and some samples have high carbonate content (e.g. M2AR 2.2, M2AR 2.3, M2AR 7.8 VII, and M2AR 7.8 XI), thus we cannot correct for Ca in carbonates to obtain CaO*. To calculate CaO*, we have assumed the value CaO = Na_2O if CaO > Na_2O (Bock et al., 1998). CIA values for unaltered plagioclase and K-feldspars typical of unaltered upper crustal rocks are approximately equal to 50, whereas higher CIA values represent higher degrees of weathering. The CIA value of the PAAS standard, representing the composition of the upper continental crust is equal to 67 (Taylor and McClennan, 1985). The grain-size sorting effect can be evaluated using the Al/Si ratio as it can be considered a proxy for sediment grain size (Bouchez et al., 2011). The sedimentary sorting effect favors heavy mineral concentrations such as zircon and quartz dilution in the coarser fraction, which could modify the trace element ratios used as provenance proxies (McLennan et al., 1993; Roddaz et al., 2014). The analyzed samples exhibit high levels of loss on ignition (LOI) ranging from 6.6 % to 42.6 %, with an average of 21.5 %. The presence of high concentrations of CaO in the Post-rift I samples (M2AR 9-1; M2AR 10.75 II; M2AR 7-8 XI; M2AR 7-8 VII; M2AR 2-3 and M2AR 2-2) may explain the high LOI concentrations. Additionally, the presence of organic material, particularly in the black shale samples (M2AR 7-8 VIII; M2AR 6-9, and M2AR 6-8), could further contribute to these high LOI, as discussed in Heiri et al. (2001) and Beaudoin (2003).

On the eastern part of the Araripe Basin, the calculated CIA value from the rift-beginning sample (M2AR 4-2, Brejo Santo Formation) is 95, much higher than those of the PAAS. The calculated CIA values for the post-rift I stage samples range from 61 to 83. On the western side, the CIA value of the post-rift II stage sample (M2AR 1-5 — Exu Formation) is 93. We were unable to calculate CIA values for the M2AR 1.3 (Araripina Formation), M2AR 2.2, and M2AR 2.3 (Romualdo Formation) samples because they have concentrations below the detection limit (Table S7 in the Supplementary data).

The rift beginning sample M2AR 4-2 (Brejo Santo Formation) has an Al/Si ratio of 0.40. The post-rift I stage samples have an Al/Si ratio between 0.10 and 0.43. On the western side, the post-rift I stage samples of the Romualdo Formation (M2AR 2-2 and M2AR 2-3) have 0.29 and 0.38 Al/Si ratio values, respectively. The post-rift II stage M2AR 1.3 (Araripina Formation) and M2AR 1.5 (Exu Formation) samples have Al/Si values of 0.53 and 0.18.

The Cr/Th ratio value of the rift-beginning stage sample M2AR 4-2 (Brejo Santo Formation) is 12.6. The Cr/Th ratios of the post-rift I stage samples range from 0.4 to 10.3 (S7 in the Supplementary data). The Cr/Th ratios of the post-rift II stage samples M2AR 1-3 (Araripina Formation) and M2AR 1-5 (Exu Formation) are 22.81 and 7.29, respectively. The Th/Sc ratio value of the rift beginning stage sample M2AR 4-2 (Brejo Santo Formation) is 0.29. The Th/Sc ratios of the post-rift I stage samples exhibit strong variations ranging from 0.32 to 1.92. The Th/Sc ratios of the post-rift II stage M2AR 1-3 (Araripina Formation) and M2AR 1-5 (Exu Formation) samples are 1.21 and 1.24, respectively.

4.1.1. Rare Earth Elements (REEs)

The Eu anomaly was calculated relative to chondrites: $Eu/Eu^* = Eu_N / (Sm_N \times Gd_N)^{1/2}$, where N refers to the chondrite-normalized concentration value (Condie, 1993). This parameter facilitates comparisons between sediments derived from basic or felsic sources (Cullers, 2000) and the PAAS (Taylor and McClennan, 1985; Pourmand et al., 2012). For instance, low Eu/Eu* ratios (0.3 to 0.94) are characteristic of felsic and silicic source rocks in fine-grained sedimentary protoliths, whereas higher Eu/Eu* ratios (0.71–1.02) of fine-grained sedimentary rocks indicate more mafic and less differentiated source rocks (McLennan et al., 1990; Cullers, 2000). The cerium anomaly (ΩCe) normalized to PAAS is calculated as follows (De Baar et al., 1985): $\Omega Ce = 2 \times (Ce_{sample} / Ce_{PAAS}) / [(La_{sample} / La_{PAAS}) + (Pr_{sample} / Pr_{PAAS})]$, where X_{sample} is the concentration of samples and X_{PAAS} refers to the concentration of the PAAS standard.

When normalized against PAAS, most analyzed samples have relatively flat REE patterns, variable Eu anomalies, and slight enrichment in Heavy REEs (HREE). The exceptions are the two samples from the post-rift II stages which are an enrichment in Middle REEs (MREE) for the sample of the Exu Formation and a depletion in MREEs for the sample of the Arapina Formation (Fig. S8 Supplementary dataset). The Ce anomaly of the rift beginning stage (M2AR 4-2 — Brejo Santo Formation) is 0.89. The post-rift stage samples have variable Ce anomalies between 0.82 and 1.45. The post-rift II stage sample of the Araripina Formation has a ΩCe value close to that of the PAAS (1.04) while the post-rift II sample of the Exu Formation has ΩCe much higher than PAAS (1.50) (Table S7 in the Supplementary data). All the analyzed values are systematically higher than those measured in authigenic smectites and seawater (Ωe < 0.50) (De Baar et al., 1985) and they do not show any variation with the stratigraphic position. There is no correlation of the Ωe ratio with REE contents, the CIA values, the Al/Si ratio, the Cr/Th ratio, the Th/Sc ratio, the Eu/Eu*, and the ε_{Nd} (0) values (Table S2, Supplementary dataset). The Eu/Eu* ratio of the rift beginning stage sample of the Bejo Santo Formation is 0.80. The post-rift I stage samples have Eu/Eu* ratios between 0.60 and 1.31. The post-rift II stage samples have a similar Eu/Eu* ratio (0.74). All analyzed samples have Eu/Eu* ratios higher than the PAAS (i.e., Eu/Eu* = 0.58) (Table 2).

4.2. Sm–Nd isotopes

The Sm–Nd isotope compositions of early Cretaceous sedimentary rocks of the Araripe Basin are presented in Table 2 and Fig. 5. Ages and the ε_{Nd} (T) values of samples were calculated based on stratigraphic ages from Assine (2007) and Fambrini et al. (2020). For the Abaiara Formation we used 140 Ma; for the Barbalha Formation, 119 Ma; for the Romualdo Formation, 113 Ma; for the Araripina Formation, 110

Table 2
Sm–Nd systematics of analyzed sedimentary rocks from Araripe Basin.

Madre de Dios	Sample	Formation	Age	Sm (ppm)	Nd (ppm)	$^{147}Sm/^{144}Nd$	$^{143}Nd/^{144}Nd$	$\pm 2\sigma$ (10^{-6})	$\varepsilon_{Nd\ (0)}$	$\varepsilon_{Nd\ (T)}$	TDM (Ga)	TDM* (Ga)
1	M2AR 04.2	Abaiara	Berriasian–Hauterivian	4.611	23.760	0.1173	0.511973	±18	−12.98	−11.6	1.68	1.68
2	M2AR 09.1	Barbalha	Aptian	5.119	26.808	0.1154	0.512008	±16	−12.28	−11.1	1.59	1.63
3	M2AR 10.75 II	Crato	Aptian	9.796	50.356	0.1176	0.511431	±3	−23.54	−22.4	2.55	2.44
4	M2AR 02.3	Romualdo	Aptian	0.821	4.811	0.1031	0.511796	±33	−16.42	−15.1	1.71	1.91
5	M2AR 06.2	Romualdo	Aptian	5.957	32.205	0.1118	0.511973	±5	−12.97	−11.8	1.60	1.67
6	M2AR 07.3	Romualdo	Aptian	6.512	35.054	0.1123	0.511640	±6	−19.47	−18.3	2.10	2.14
7	M2AR 07.6	Romualdo	Aptian	11.091	68.069	0.0985	0.511430	±6	−23.57	−22.2	2.12	2.43
8	M2AR 01.3	Araripina	Albian-Cenomanian	0.834	6.518	0.0774	0.511422	±13	−23.72	−22.1	1.80	2.42
9	M2AR 01.5	Exu	Albian-Cenomanian	34.019	189.053	0.1088	0.511673	±16	−18.82	−17.7	1.98	2.09

Ages and the εNd (T) values of samples were calculated based on stratigraphic ages from Assine (2007) and Fambrini et al. (2020). For Abaiara Formation we used 140 Ma; for Barbalha Formation, 119 Ma; for Romualdo Formation, 113 Ma; for Araripina Formation, 110 and for Exu Formation, 100 Ma.

and for the Exu Formation, 100 Ma. The rift beginning stage sample has an ε_{Nd} (0) value of −13.0, and ε_{Nd} (T) value of −11.6. Its $T_{DM\ (0)}$ age is 1.68 Ga and its $T_{DM\ (*)}$ age is 1.68 Ga. The post-rift I stage sample of the Barbalha Formation has an ε_{Nd} (0) value of −12.3, ε_{Nd} (T) value of −11.1, $T_{DM\ (0)}$ age of 1.59 Ga and $T_{DM\ (*)}$ age of 1.63 Ga. Other post-rift I stage samples have lower ε_{Nd} (0) values between −16.4 and −23.6, lower ε_{Nd} (T) values between −11.8 and −22.4, and older $T_{DM\ (0)}$ and $T_{DM\ (*)}$ ages (Table 2). The analyzed samples of the post-rift II stage have variable ε_{Nd} (0) and ε_{Nd} (T) values, lower than those of the beginning rift and Barbalha Formation samples but within the range of those of other post-rift I stage samples. They have also older $T_{DM\ (0)}$ and $T_{DM\ (*)}$ ages than those of the beginning rift and Barbalha Formation samples (Table 2).

4.3. Detrital zircon

4.3.1. U–Pb geochronology

The U–Pb zircon ages of the analyzed Mesozoic sedimentary rocks of the Araripe Basin are presented in Table 3 and Fig. 6. Individual analysis can be found in the Supplementary dataset. For simplification, the U–Pb zircon age distribution of each analyzed sample was grouped into the four tectonic stages that defined the tectonic evolution of the Araripe Basin during the Mesozoic: the rift-beginning stage, the rift stage, the post-rift I stage, and the Post-rift II stage.

The U–Pb zircon age distribution of the rift beginning stage sample is dominated by Paleoproterozoic ages (2.5–1.6 Ga) (40 %), especially Rhyacian–Orosinian (2.3–1.8 Ga) ages (33 %). Subordinate zircon populations include 25 % of Neoproterozoic ages (1.0–0.54 Ga), and 23 % of Mesoproterozoic ages (1.6–1.0 Ga). The Archean age (>2.5 Ga) grains represent 8.5 % and Paleozoic/Mesozoic age (<541 Ma) grains are 3.5 %. The U–Pb zircon age distribution of the rift stage sample is dominated by Neoproterozoic ages (1.0–0.54 Ga) (38 %), especially Ediacaran ages (635–541 Ma) (19 %). Subordinate zircon populations include 32 % of Paleoproterozoic and 14 % of Mesoproterozoic zircon ages. The Paleozoic/Mesozoic age (<541 Ma) grains are 9 %, and Archean age (>2.5 Ga) grains represent 7 %. The U–Pb age distribution of the post-rift I stage samples is dominated by Paleoproterozoic ages (2.5–1.6 Ga) (53.3 %), especially Rhyacian (2.3–2.0 Ga) (24.5 %), and Statherian (1.8–1.6 Ga) zircon ages (18 %). Subordinate zircon populations include 31.2 % of Neoproterozoic ages (1.0–0.54 Ga), and 7.6 % of Archean ages (>2.5 Ga). The Mesoproterozoic ages (1.6–1.0 Ga) represent 4.4 % and Paleozoic/Mesozoic age (< 541 Ma) grains are 3.5 %. The proportion of Stenian–Tonian (1.2–0.7 Ga) zircon strongly decreases in the U–Pb age distribution of the post-rift I samples compared to that of the rift stage samples. The U–Pb age distribution of the post-rift II stage is dominated by Neoproterozoic ages (1.0–0.54 Ga) (46.4 %), especially Ediacaran (635–541 Ma) zircon ages (41 %). Subordinate zircon populations include Paleoproterozoic ages (2.5–1.6 Ga) (33.2 %), Paleozoic/Mesozoic ages (<541 Ma) (11.7 %), and Archean ages (>2.5 Ga) (6.7 %).

In addition to the concordant zircon ages described above, all the analyzed samples contain a significant proportion of discordant zircon ages. The rift beginning sample and the rift sample show discordant grains with upper intercepts between 2.0 and 2.4 Ga and lower intercepts around 0.48 Ga (Fig. S6 in Supplementary data). The post-rift I sample has upper intercepts between 2.2 and 1.9 Ga and lower intercepts between 0.5 and 0.19 Ga, respectively (Fig. S6 in Supplementary data). The post-rift II of the Exu Formation has an upper intercept at 2.3 Ga and a lower intercept at 0.48 Ga (Fig. S6 in Supplementary data). Finally, the trace element concentrations of concordant and discordant zircon from the Araripe Basin show similar characteristics (Fig. S6 in Supplementary data). Most grains are plotted in the continental arc field, which suggests a main contribution from old continental crust. However, some zircon grains, generally from the Ediacarian (0.63–0.54 Ga), Calymmian (1.6–1.4 Ga), and Rhyacian (2.3–2.0 Ga) ages, plotted in the mid-ocean ridge field (Fig. S6 in supplementary data), which suggest some juvenile contribution.

4.3.2. Morphology

The results of the zircon morphological analysis are summarized in Table 4 and illustrated in Figs. 8 and 9. The analyzed zircon grains generally have mean lengths of 70 μm and 230 μm. The rift-beginning stage sample (M2AR 4.1) contains 78 % subangular to subrounded, 17 % rounded, and 5 % euhedral grains. In terms of elongation, 41 % are oval, 33 % are elongated, and 25 % are round grains. The rift stage sample (M2AR 5.1) contains 66 % subangular to subrounded, 18 % rounded, and 17 % euhedral grains. In terms of elongation, 46 % are oval, 37 % are elongated, and 17 % are round grains. The post-rift I samples (M2AR

Table 3
Numbers and percentages (%) of U–Pb ages.

Time (Ma)	Age	Geological framework	Rift-beginning		Rift		Post-rift I		Post-rift II	
			Number	%	Number	%	Number	%	Number	%
145.0–100.5	Early Cretaceous	1 — Parnaíba Basin[b]					1	0.10 %		
251.9–145.0	Jurassic/Triassic		1	0.50 %	1	0.60 %			1	0.40 %
298.9–251.9	Devonian		1	0.50 %						
358.9–298.9	Carboniferous		2	1.00 %	1	0.60 %	3	0.40 %		
419.2–358.9	Devonian						1	0.10 %		
443.8–419.2	Silurian		1	0.50 %			2	0.30 %		
485.4–443.8	Ordovician	2 — Felsic dykes (ca. 460 Ma)[a]					3	0.40 %	1	0.40 %
541.0–485.4	Cambrian	3 — Brasiliano Orogeny (620–510 Ma)[a]	2	1.00 %	12	7.60 %	17	2.20 %	28	10.90 %
635–541	Ediacaran		27	13.70 %	31	19.50 %	167	21.30 %	105	41.00 %
720–635	Cryogenian	4 — Metavulcanosedimentary belts (mostly <650 Ma)[a]	16	8.10 %	13	8.20 %	47	6.00 %	7	2.70 %
1000–720	Tonian	5 — Ophiolite complexes (820–650 Ma)[a]	6	3.00 %	17	10.70 %	31	3.90 %	7	2.70 %
1200–1000	Stenian	Tonian rift-related rocks (900–860 Ma) Cariris Velhos Event (1000–920 Ma)	15	7.60 %	17	10.70 %	22	2.80 %	2	0.80 %
1400–1200	Ectasian		27	13.70 %	4	2.50 %	9	1.10 %	2	0.80 %
1600–1400	Calymmian	7 — Paleo/Mesoproterozoic rift-related plutons (ca. 1.7–1.5 Ga)	3	1.50 %	1	0.60 %	4	0.50 %	1	0.40 %
1800–1600	Statherian	Oros-Jaguaribeano Belt (ca. 1.8–1.7 Ga)[a]	9	4.60 %	1	0.60 %	141	18.00 %	13	5.10 %
2050–1800	Orosinian	8 — Paleoproterozoic basement units[a]	34	17.30 %	19	12.00 %	73	9.30 %	37	14.40 %
2300–2050	Rhyacian		31	15.70 %	29	18.20 %	192	24.50 %	32	12.50 %
2500–2300	Siderian		5	2.50 %	2	1.30 %	12	1.50 %	3	1.20 %
2800–2500	Neoarchean	9 — Archean nuclei inliers[a]	12	6.00 %	10	6.30 %	45	5.70 %	13	5.10 %
3200–2800	Mesoarchean				1	0.60 %	3	0.40 %	2	0.80 %
3600–3200	Paleoarchean		5	2.50 %			12	1.50 %	2	0.80 %
Total grains			**197**	100 %	**159**	100 %	**785**	100 %	**256**	100 %

[a] Geological framework of Borborema Province described by Caxito et al., 2020.
[b] Geological framework of Parnaíba Basin based on Vaz et al., 2007 and Assis et al., 2019.

Table 4
Zircon statistics. Grains with length/width ratios of 1.3–1.8 are oval, grains with higher and lower ratios are elongated (Elon) and round (Rou), respectively; euh = euhedral, ro = rounded, sa–sr = subangular to subrounded.

Sample	Formation	Age	Shape (%)			Roundness (%)			# of concordant/total ages	Mean (interval of) grain length (μm)
			Elon	Oval	Rou	Euh	Sa–sr	Ro		
M2AR 01.4	Exu	Albian–Cenomanian	39	37	24	10	68	22	41/106	92 (60–172)
M2AR 01.3	Araripina	Albian	41	16	42	29	66	5	111/126	135 (65–211)
M2AR 06.1	Romualdo	Aptian	69	25	6	26	69	4	117/129	236 (104–416)
M2AR 06.9	Romualdo	Aptian	56	30	15	18	72	10	61/113	103 (38–184)
M2AR 07.2	Romualdo	Aptian	57	28	15	20	61	18	93/122	113 (53–219)
M2AR 07.5	Romualdo	Aptian	59	25	16	31	59	10	51/126	167 (93–284)
M2AR 10.I	Crato	Aptian	73	18	10	10	82	8	62/110	119 (59–204)
M2AR 11.1	Barbalha/Crato	Aptian	51	37	11	29	67	4	70/109	156 (60–344)
M2AR 08.1	Barbalha base	Aptian	52	33	15	9	80	10	87/128	150 (62–310)
M2AR 05.1	Abaiara	Berriasian–Hauterivian	37	46	17	16	66	18	82/110	147 (66–259)
M2AR 04.1	Brejo Santo	Jurassic	33	41	25	5	78	17	63/124	100 (62–180)

8.1, M2AR 11.1, M2AR 10I, M2AR 7.5, M2AR 7.2, M2AR 6.9, and M2AR 6.1) contain 59 %–80 % subangular to subrounded, 18 %–4 % rounded, and 31 %–9 % euhedral grains. In terms of elongation, 18 %–37 % are oval, 73 %–51 % are elongated, and 16 %–6 % are round grains.

5. Discussion

5.1. Influence of weathering, authigenesis, and anoxic conditions on provenance proxies

The Eu anomalies expressed as Eu/Eu*, elemental ratios (Cr/Th, Th/Sc, Zr/Sc), and Sm–Nd isotopic compositions of sedimentary rock have proven to be useful tools for determining the provenance of ancient sediments (McLennan et al., 1993). For instance, low Eu/Eu* ratios (0.3 to 0.94), high Th/Sc (>0.64), and low Cr/Th (<15) of fine-grained sedimentary rocks are characteristic of felsic and silicic source rocks, whereas higher Eu/Eu* ratios (0.71–1.02), higher Cr/Th (>22), and lower Th/Sc (<0.4) of fine-grained sedimentary rocks suggest more mafic and less differentiated source rocks (McLennan et al., 1993; Cullers, 2000). However, before determining the provenance of the analyzed sedimentary rocks, it is important to evaluate the effects of grain-size sorting and diagenesis, on trace element ratios, and REE concentration of the analyzed sedimentary rocks.

The grain-size sorting effect can be evaluated using the Al/Si ratio as it can be considered as a proxy for sediment grain size (Bouchez et al., 2011). The sedimentary sorting effect favors the concentration of quartz and heavy minerals like zircon in the coarser fraction (McLennan et al., 1993; Roddaz et al., 2014). The samples M2AR 4-2; M2AR 6.8BS; M2AR 6-9BS; M2AR 7-3; M2AR 7-6; M2AR 7.8VII; M2AR 7-8VIII; M2AR 7-8XI; M2AR 7-8 XXII; M2AR 2-2; M2AR 2-3; M2AR 1-3, and M2AR 9-1 have high Al/Si ratios (0.29–0.53) (Table S7 in the Supplementary data, Fig. 5), suggesting a high concentration of fine and clay-rich sediments (Bouchez et al., 2011). The samples M2AR 7-7; M2AR 6-3; M2AR 7-5BS; M2AR 7-4; M2AR 1-5; M2AR 6-2; and M2AR 10-75II have low Al/Si ratios (0.10–0.24), suggesting that these samples are enriched in quartz. There is no correlation of the Al/Si ratio with the REE content, Eu/Eu*, Cr/Th, Th/Sc, and ε_{Nd} (0) (see Table S2 in the Supplementary dataset), which indicates that sedimentary sorting has not modified these provenance proxies.

Diagenesis can promote the remobilization of Eu under reducing conditions (MacRae et al., 1992). These processes can modify the REE patterns, the Eu/Eu*, and Cr/Th ratios (Tribovillard et al., 1996). Compared to PAAS, authigenic smectites formed in deep-water environments are characterized by LREE depletion, HREE enrichment, and strong negative Ce anomalies (ΩCe < 0.50, De Baar et al., 1985). Most samples from the Araripe Basin, mainly the post-rift I samples have Ce anomalies (ΩCe) higher than 0.80 (Table S7 in the Supplementary data) indicating that authigenic smectites were not incorporated during the early diagenetic process. These samples have flat REE patterns against PAAS corresponding to the "shale" field (Fig. 4), typical of continental clays (see Moiroud et al., 2016), and hence are not influenced by authigenesis. The sample M2AR 4-2 from the rift-beginning stage, and the sample M2AR 2-3 from the post-rift I stage are enriched in HREEs over LREEs and plotted between the "shale" and "seawater" fields (Fig. 4). They both have ΩCe > 0.80 suggesting that the formation of authigenic smectites if occurred was a minor process. The low Eu/Eu* ratio values suggest that the diagenetic remobilization of Eu under reducing conditions was negligible in the analyzed samples.

In the rift-beginning stage, the sample M2AR 4-2 presents low Th/Sc values (0.3), low Th/Cr (0.05), and high Eu/Eu* ratios (0.8), which suggest trace element ratios typical of "basic" sediments (Table S7 in the Supplementary data, Fig. 5), whereas in the post-rift I and post-rift II stages all the samples show felsic and silicic parameters. Three samples (M2AR 4-2, 7-5, and 7-8 VII) present high Eu/Eu* ratios (0.8–1.3). The positive Eu anomaly in the post-rift I stage (M2AR 7-5, and 7-8 VII) could be explained by the remobilization of Eu under reducing conditions, as suggested by geochemical and paleontological proxies onto

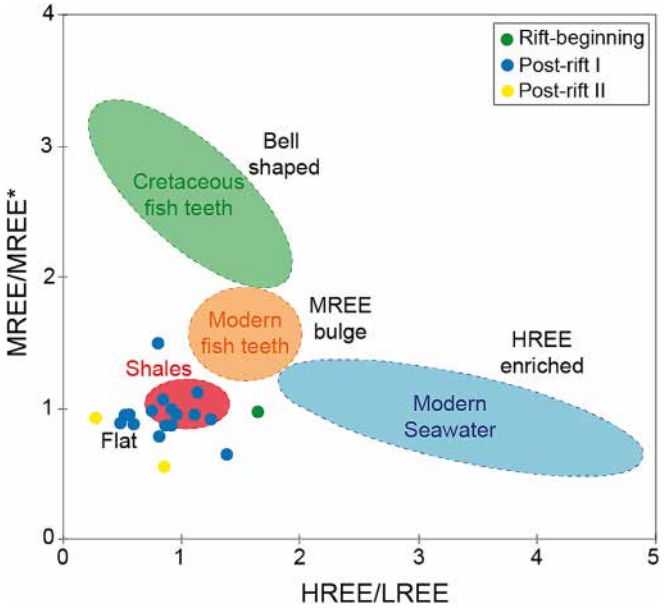

Fig. 4. HREE/LREE vs. MREE/MREE* diagram. HREE/LREE and MREE/MREE* values are calculated following Martin and Scher (2004), where HREE = Tm + Yb + Lu, LREE = La + Pr + Nd, MREE = Gd + Tb + Dy (all PAAS normalized), and MREE* = the average of HREE + LREE. The MREE bulge and "bell-shaped" REE profiles correspond to REE patterns observed in fish teeth, Fe–Mn oxides, organic matter, and pore waters, while "HREE-enriched" profiles correspond to modern seawater (Huck et al., 2016; Moiroud et al., 2016). These end-members reflect the REE contents of marine sediments influenced by seawater or authigenic phases, while "flat" REE patterns are characteristic of continental clays (see Huck et al., 2016; Moiroud et al., 2016 for a review).

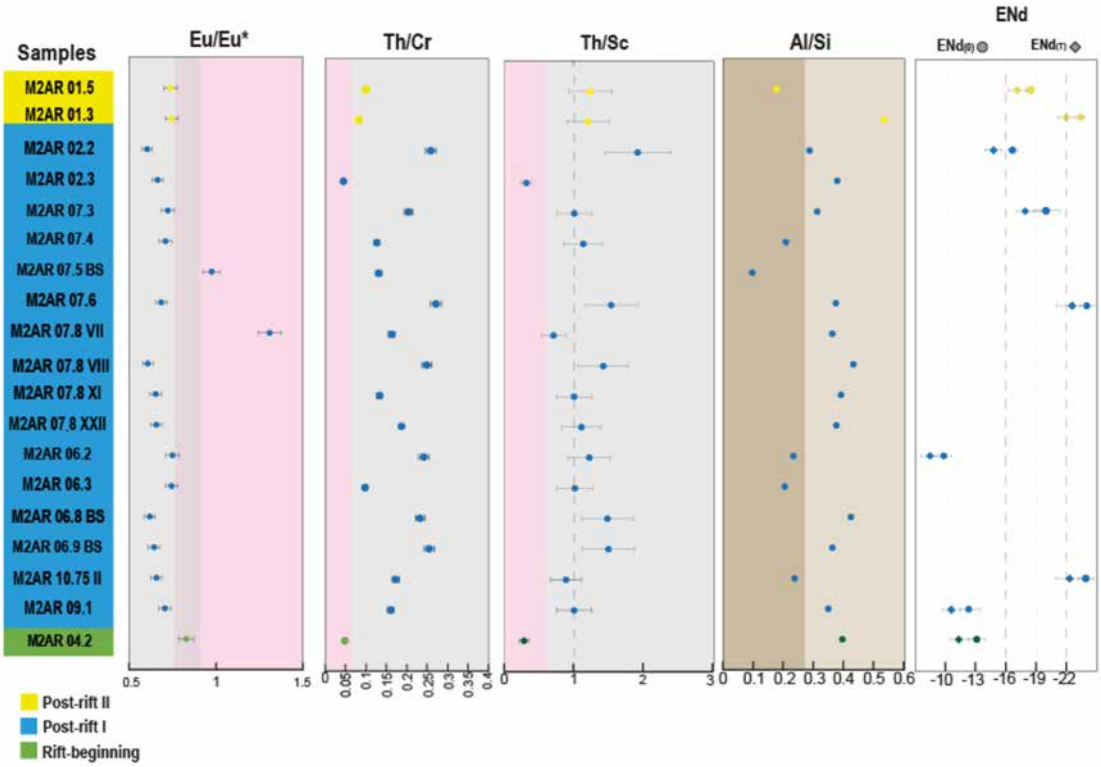

Fig. 5. Stratigraphic variation of the Nd isotope composition (expressed as εNd(0)/ for the round points, and εNd(T)/ for the rhombus points). The lengths of the horizontal bar for the Sm–Nd isotopic compositions correspond to 2σ analytical errors (see Table 2). Selected trace element ratios (Eu/Eu*, Th/Cr; Th/Sc and, Al/Si see text for details) of analyzed samples (green points — Rift stage; blue points — Post-rift I stage; yellow points — Post-rift II stage). The horizontal bars for the Eu/Eu*, Th/Cr, and Th/Sc, ratios correspond to 5 % (i.e., the Eu concentration analytical error, see Supplementary material), 15 % (i.e., the sum of the Cr and Th concentration analytical errors), and 25 % (i.e., the sum of the Th and Sc concentration analytical errors). Pink and gray rectangles indicate the value range for basic and felsic sediments, respectively (Cullers, 2000).

the Romualdo Formation (i.e. Sobradinho section in Bom et al., 2021). The low Eu/Eu* ratio values suggest that the diagenetic remobilization of Eu under reducing conditions was negligible in the rest of the analyzed samples. The REE concentrations of the post-rift II analyzed samples (M2AR 1-3 and M2AR 1-5) against PAAS show contrasting patterns. The samples plot outside of the shale field suggesting that the REE concentrations have been perturbed by post-depositional processes (see Supplementary dataset Fig. S8). M2AR 1-5 shows a strong enrichment in HREEs (Fig. S8) that could be associated with a primary phase of the pedologic process. In a study of the lateritic process in a tropical environment, Viers and Wasserburg (2004) indicated that the Zr dispersion could elevate the HREE concentrations at the early stage of the weathering process, and the Zr could remove the REEs during that phase explaining the HREE enrichment, for the sample. However, the provenance proxies of the other analyzed samples were not affected by the effects of grain-size sorting and the diagenesis process.

5.2. Provenance interpretations

The εNd (0) values (−12.3 to −23.7) together with the T_{DM} ages (1.68 to 2.55 Ga) suggest an old crustal source for all the sedimentary rocks analyzed in the Araripe Basin (Table 2, Fig. 5). Proximal terrains, such as the São José do Caiano and Açude Coremas have negative εNd (0) values (−6.3 and −28.4) and T_{DM} ages between 1.8 and 2.6 Ga (de Brito Neves and Passarelli, 2020) (Table 1). Distal areas, such as Médio Coreaú and Ceará Central Domains (Fig. 1) also present T_{DM} ages between 1.6 and 2.5 Ga, and negative εNd (t = crystallization) (between +0.5 and −25.8) (Santos et al., 2008; Arthaud et al., 2015). The Eu/Eu* and Th/Sc ratios of mainly the sedimentary rocks analyzed suggest a felsic and silicic source, with the exception of the rift-beginning sample (M2AR 4.2) which presents some contribution of a basic source (Fig. 5).

The U–Pb zircon age distribution of the analyzed samples indicates multiple sediment sources. The significant presence of Rhyacian to Orosirian (2.3–1.8 Ga), and Ediacaran (0.63–0.54 Ga) ages is the common feature among all tectonic stages. These zircon ages can be found in other places of the Borborema province (Fig. 1, Table 1). The discordant detrital zircon grains may provide additional information about the source and the influence of the Brasiliano cycle in the Borborema Province. In all stages (except in the Araripina Formation sample — M2AR 1-3), the upper intercept indicates Paleoproterozoic sources (2.2–1.8 Ga) and the lower intercept indicates the crystallization of Cambrian–Ordovician (489–460 Ma) post-orogenic granites (see Supplementary dataset Fig. S6).

Additional constraints can be obtained from the MDS graph (Fig. 7), which represents statistically the degree of similarity in U–Pb zircon age distribution between analyzed samples (Vermeesch, 2013, 2018). In this map (Fig. 7), alike samples cluster closely together and are linked by solid and dashed lines (closest and second-closest neighbors), whereas "dissimilar" samples plot far apart. In the MDS map (Fig. 7), the rift beginning and rift samples plot apart suggesting different sources for these stages. The U–Pb age distribution of the post-rift I stage is connected with dashed lines with those of the rift-beginning and rift stages suggesting common sources. The U–Pb age distribution of the post-rift II stage is connected by solid lines to other U–Pb distributions suggesting similar sources.

The main peak ages (2.3 to 1.8 Ga, 33 %, and 0.72 to 0.54 Ga, 22 %) (Fig. 6, Table 3) during the beginning of the rift (Brejo Santo and Missão Velha formations — 152–145 Ma) may be sourced by the Borborema Province. The sources of Paleoproterozoic grains could be represented by supracrustal rocks from São Pedro, São José do Caiano, Açude Coremas terranes (2.1–2.2 Ga), and Caicó Complex (São Padro terrane 2.15–2.2 Ga) from the Central sub-province; and the Orós-Jaguaribe Terrane (2.2–1.7 Ga) from the Northern sub-province (Parente and Arthaud, 1995; Hollanda et al., 2011; de Brito Neves and Passarelli, 2020). The Cryogenian–Ediacaran (0.72–0.54 Ga) (22 %, Table 3) may have been sourced by the Brasiliano (0.7–

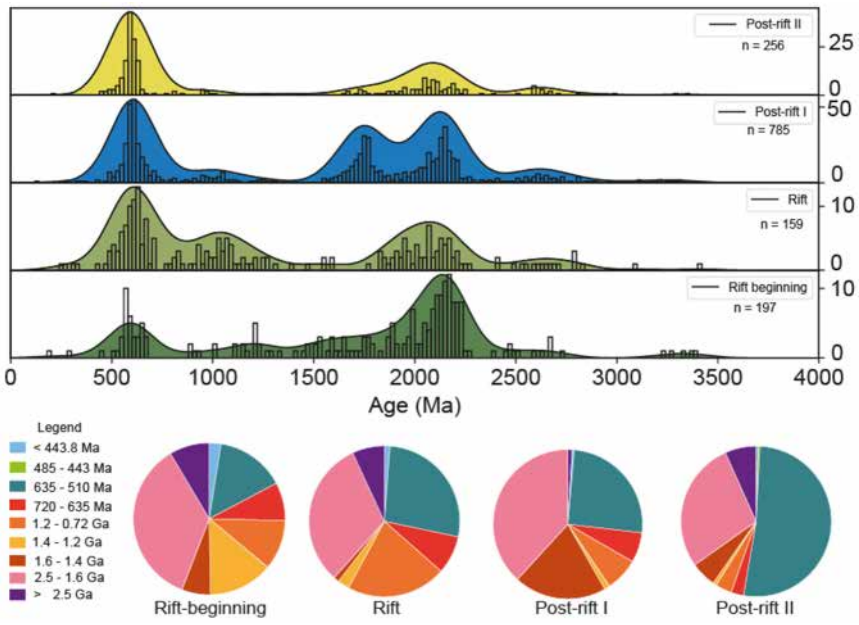

Fig. 6. Stage evolution of the U–Pb zircon age distribution of the Araripe Basin with the age probability (KDE, black line) and age histogram (bars). The lithology and age repartition of the pie charts are given in Table 3.

0.55 Ga) granitoids and metavulcanosedimentary belts that are widespread in the Borborema Province (Ferreira et al., 1998; de Brito Neves et al., 2003; Costa et al., 2013). The Rio Salgado belt rocks could also have been a source of recycled sediments, because they have pre brasiliano igneous intrusions (ca. 780 Ma), Ediacaran (635–541 Ma), and Tonian (ca. 940 Ma) detrital zircon grains (de Brito Neves and Campos Neto, 2016). Zircon grains younger than 450 Ma could be associated with post-orogenic granites (Amaral et al., 2017), however, they may also have come from recycled sediments (Parnaíba Basin; Mauriti Formation?) given the low number of zircons of this age (<4 %, Table 3). In the Southern sub-province, the Riacho do Pontal Domain presents supracrustal sequences with Paleoarchean ages up to 3.5 Ga, Paleoproterozoic ages (2.2–2.0 Ga); and volcano-sedimentary sequences with late Tonian to Ediacaran ages (820–530 Ma) (Caxito et al., 2017). However, the analyzed samples do not have a significant percentage of Tonian grains (3 %, Table 3), which suggests that there is no significant source from the eastern Central sub-province (Piancó-Alto Brigida and Alto-Pajeú Domain, Figs. 1, 6) and the internal zone of the Riacho do Pontal Domain, Southern sub-province (Fig. 1). The paleocurrent data of the Missão Velha and Brejo Santo formations indicate S–SE paleo directions (Assine, 1994, 2007; Fambrini et al., 2013; Godot Souza et al., 2022), and suggest a sedimentary provenance of the northern terranes.

The rift stage (Abaiara Formation) occurred during the Neocomian (145–130 Ma). The associated sedimentary rocks are characterized by a significant population of U–Pb zircon ages between 2.3 and 1.8 Ga (30 %), 1.2 and 0.72 Ga (22 %), and 0.72 and 0.54 Ga (28 %) (Table 3, Fig. 6). The Paleoproterozoic grains could be sourced by supracrustal rocks from the São José do Caiano and Açude Coremas terranes (2.1–2.2 Ga) placed in the Central sub-province; and, the Caicó Complex (São Padro terrane 2.15–2.2 Ga) and Orós-Jaguaribe Terrane (2.2–1.7 Ga) localized the Northern sub-province, similarly to what occurred during the rift beginning stage (Fig. 10). Similarly, the Cryogenian and Ediacaran zircons (0.7–0.55 Ga) may have been sourced by the Brasiliano granitoids and metavulcanosedimentary belts (Ferreira et al., 1998). The main difference between the rift-beginning stage samples is the abundance of Stenian–Tonian age (1.1–0.72 Ga) detrital zircon grains (Table 3, Fig. 6), which we interpret to indicate a change in the source areas during the deposition of sedimentary rocks of the rift stage. The Piancó-Alto Brigida and Alto-Pajeú Domain (de Brito Neves et al., 2005) present rocks from the Cariris Velhos cycle (970–960 Ma) with an overprint of 550–510 Ma Brasiliano granitoids (de Brito Neves et al., 2005). In the Internal Zone of the Riacho do Pontal Domain, it is also possible to find 1000–960 Ma plutonic rocks (Kozuch, 2003; Santos et al., 2010) related to the same tectonic event (Caxito et al., 2017). There are different interpretations of paleoflow during the deposition of sedimentary units from the rift stage. Godot Souza et al. (2022) indicated paleocurrents toward the south; Fambrini et al. (2019) suggested paleoflow to the north toward the Iguatu and Rio do Peixe basins, whereas Assine (1994, 2007) suggested paleoflows to SSW. The abundance of Stenian–Tonian (1.2–0.72 Ga) zircon grains (22 %, Table 3) suggests a dominant source located in the eastern terranes (Fig. 10), which is supported by the paleocurrent direction found by Assine (1994, 2007).

The analyzed samples of the Aptian first post-rift I stage (Barbalha, Crato, and Romualdo formations) contained a significant population of U–Pb Paleoproterozoic ages, between 2.3 and 1.6 Ga (52 %, Table 3) and Neoproterozoic ages (720–541 Ma) (27 %, Table 3). This post-rift I stage does not present an important percentage of Tonian detrital zircons, which we interpret to suggest a decrease of sedimentary input from the eastern terranes of the Central sub-province (Rio Gravatá and Alto-Pajeú Domain) (Fig. 1) when compared with the rift sequence. The increase of Paleoproterozoic zircon ages, mainly Statherian (1.8–1.6 Ga) grains, suggests a major contribution from the Northern sub-province (Stathenian belts in the Ceará Domain and Alto Moxotó subdomain) (Lages et al., 2019). Additionally, the paleoflows to the SE of the sedimentary rocks of the Barbalha Formation (Assine, 1994; Fambrini et al., 2019, 2020; Godot Souza et al., 2022) might suggest a contribution from the Orós-Jaguaribe Terrane, but also from the Ceará Domain, which has a Paleoproterozoic basement and plutonic suits (2.3–2.1 Ga), Neoproterozoic granites (640–560 Ma), and Brasiliano molasses rocks (530 Ma) (Fetter et al., 2000; Arthaud et al., 2015), and recycled sedimentary from the Parnaíba Basin (Hollanda et al., 2018). The Albian–Cenomanian sedimentary rocks of the second post-rift phase ("post-rift II", Araripina and Exu formations) are characterized by a significant increase of Cryogenian–Ediacaran U–Pb ages (720–541 Ma) (44 %) and an important percentage of Paleoproterozoic ages (2.3–1.6 Ga) (32 %) (Table 3). The Araripina Formation was deposited in the western part of the Araripe Basin in the basement (Assine, 2007; Fambrini et al., 2020). The M2AR 1-3 sample has 85 % of Neoproterozoic ages (720–541 Ma), which could come from proximal sources, such as São Pedro Terrane (Fig. 1), where there are Brasiliano plutons (de Brito Neves et al., 2023). The

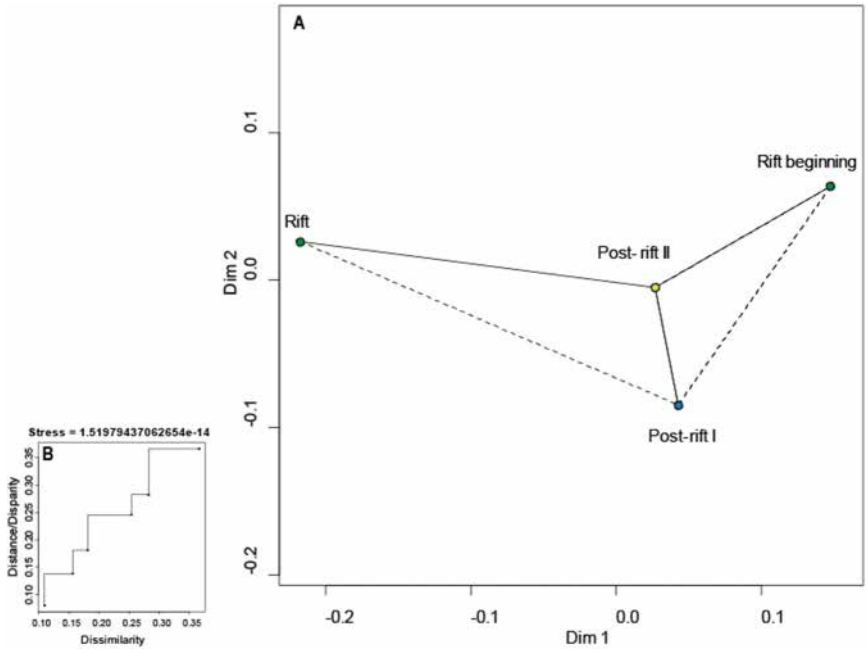

Fig. 7. A) Non-matrix metric multi-dimensional scaling (MDS) plot (Vermeesch, 2013) based on the U–Pb age distributions of detrital zircons in the analyzed samples using the Kolmogorov–Smirnov test. Closest and second closest neighbors are linked by solid and dashed lines, respectively; B) Shepard plot of the U–Pb data showing the transformation from dissimilarity to distances and disparities.

Paleoproterozoic ages (2.3–1.6 Ga) and the subordinary Archean ages (3.6–2.5 Ga) are present only in the Exu Formation sample (M2AR 1-4), and may have come also from São Pedro Terrane ("Granjeiro Complex", de Brito Neves and Passarelli, 2020). However, the paleoflow of the Exu Formation indicates a direction to the W–SW (Assine, 1994; Godot Souza et al., 2022 and this study, see Supplementary material Fig. S1), which suggests a change of the sedimentary sources from NW to NE. In this scenario, the sources of the Araripina Formation may have come from proximal terranes, as discussed above, and the Exu Formation sample may have come from the eastern part of Orós Jaguaribe Terrane (Seridó–Jaguaribe domain, Hollanda et al., 2011), which had a "long-lived Paleoproterozoic magmatic history" (Hollanda et al., 2011).

Overall, the zircon grains exhibited a diverse range of lengths, and most were categorized as oval and elongated (Fig. 9). These characteristics suggest that most of the zircon grains were from a first-cycle sediment transport and less expressed recycling (meta)sedimentary units (Augustsson

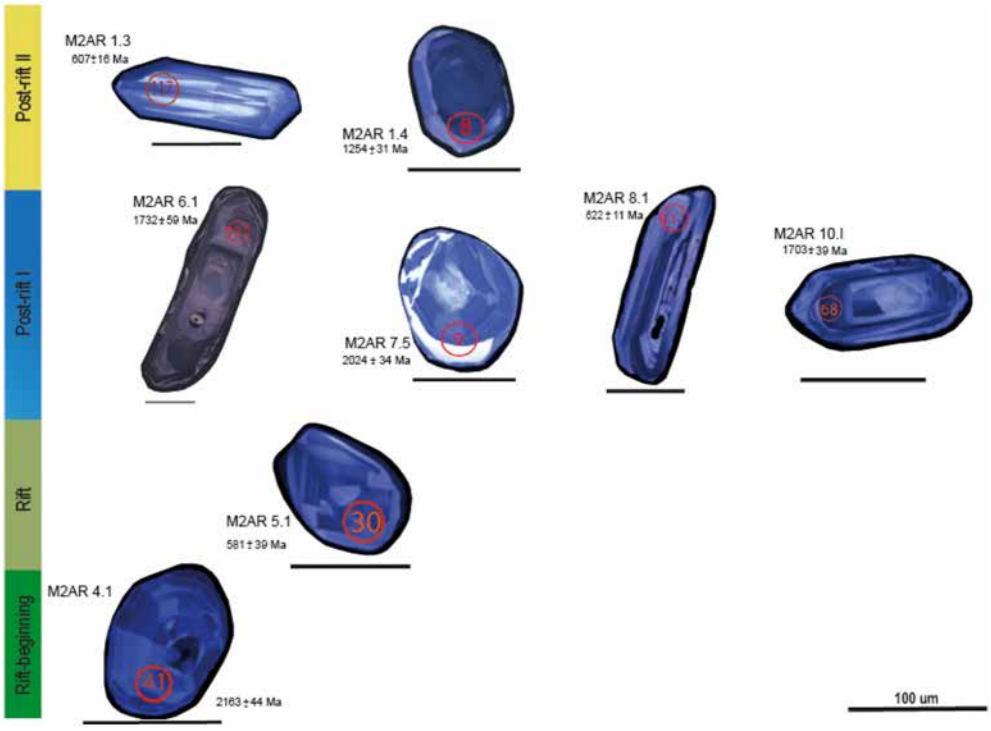

Fig. 8. Cathodoluminescence images of selected grains with different ages, roundness, and elongation. Rift-beginning stage: M2AR 4.1, Rift stage: M2AR 5.1, Post-rift I stage: M2AR 8.1, M2AR 10.I, M2AR 6.1, M2AR 7.9; Post-rift II stage: M2AR 1.3 and M2AR 1.4.

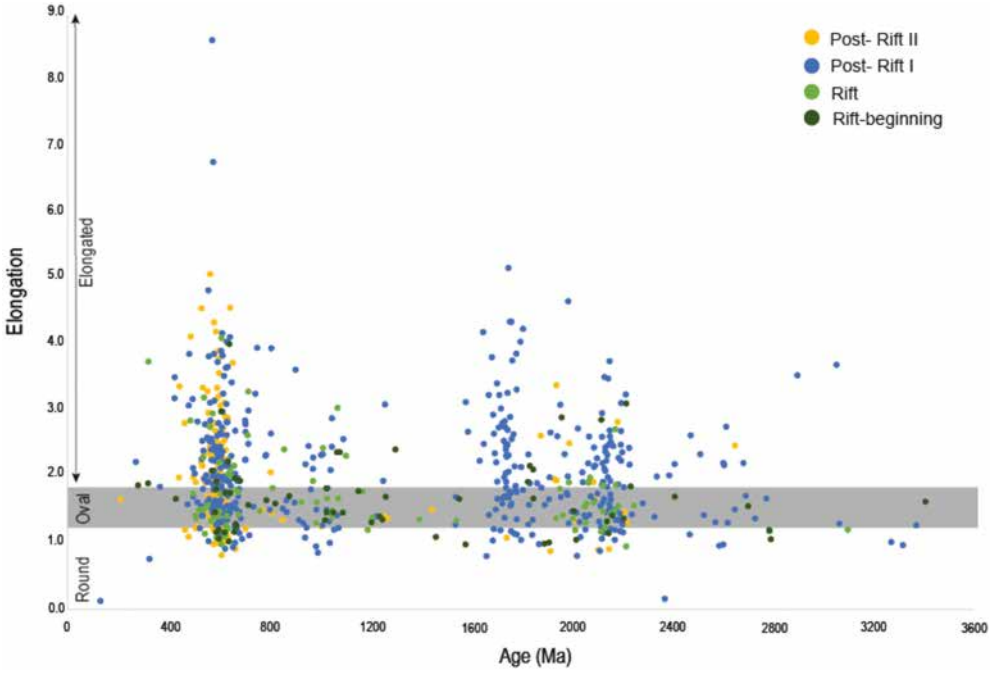

Fig. 9. Detrital zircon elongation vs. concordant age. The field for oval grains (length/width = 1.3/1.8) is marked by a horizontal gray bar. Broken grains without a clear shape in the cathodoluminescence images were not included.

et al., 2018). We investigated the correlation between zircon shape, U–Pb ages, and potential zircon-producing events. The dominant zircon populations — Rhyacian to Orosirian (2.3–1.8 Ga), and Ediacaran (0.63–0.54 Ga) are present in both oval and elongated shapes across all the stages. This suggests that sedimentation sorting did not influence the U–Pb zircon age distribution and emphasizes the dominant

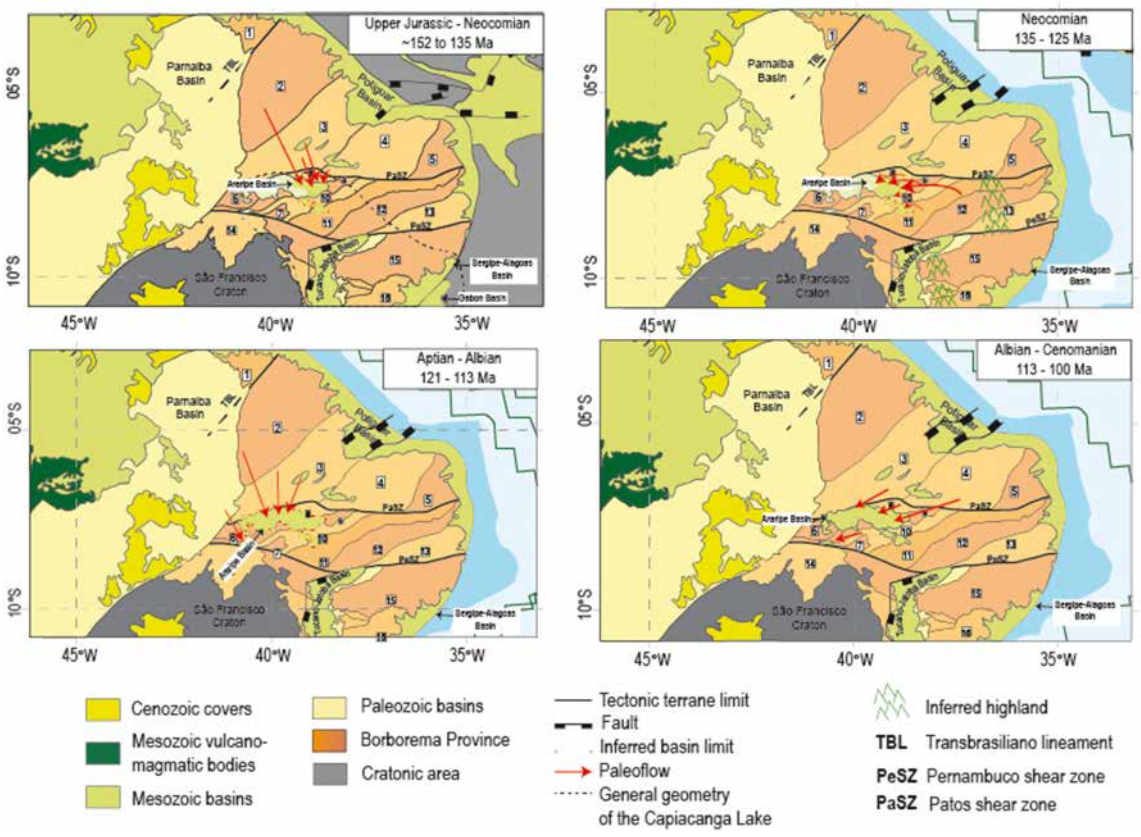

Fig. 10. Schematic paleogeographic maps based on sample provenance interpretations. Each time step corresponds to one of the tectonic stages that affected the Araripe Basin between the late Jurassic and the Cenomanian. The paleogeographic reconstruction is based on the kinematic model of Heine et al. (2013), and the paleogeographic maps from Godot Souza et al. (2022), and Matos et al. (2021a, 2021b). The Borborema Province sub-divisions and their references are listed in Fig. 1. The Capianga Lake geometry (Map A) and the highland location in Map B were based on Kuchle et al. (2011). The paleoflow directions were based on data from Fambrini et al. (2019), Assine (1994, 2007), Custódio et al. (2017), Godot Souza et al. (2022), and this study.

contribution of the Borborema Province basement and the Brasiliano granitoid plutons.

5.3. Paleogeographic implications

Our provenance dataset brings new constraints on the paleogeographic evolution of the Araripe Basin and to a larger extent, to the northern part of the South American platform from the Jurassic to the Cenomanian.

During the late Jurassic–Neocomian times (152–139 Ma), the Araripe Basin was part of the so-called Afro-Brazilian (Garcia and Wilbert, 1995; Assine, 2007; Kuchle et al., 2011) depression formed in response to early rifting caused by lithospheric stretching of the central and northern Gondwana before the breakup (Assine, 2007; Kuchle et al., 2011; Scherer et al., 2014; Guzmán-González et al., 2020). During this period, the Brejo Santo and Missão Velha formations of the Araripe Basin were deposited (Assine, 2007; Fambrini et al., 2020) and were part of the basal sequence (SEQ-1) that characterized the first infilling stage of the Afro-Brazilian depression (Dom João Stage, Kuchle et al., 2011). This basal sequence (SEQ-1) is characterized by Capianga Lake lacustrine deposits (Kuchle et al., 2011) that extend through the Recôncavo, Tucano, Jatobá, Araripe, Sergipe, Alagoas, and Gabon basins (Fig. 10). This Afro-Brazilian depression had a depocenter in the Recôncavo–Tucano–Jatobá Basin and no evidence of internal structural high that could have compartmentalized the depression is found (Kuchle et al., 2011). Our provenance data further suggest that the source area during the early rift stage (SEQ-1) was located in the northern and northwestern terranes of the Borborema (Fig. 10, Table 1). This agrees with the hypothesis of Assine (1994), who suggests a source located in the basement block localized toward the north, near the Parnaíba lineament (Patos shear zone) based on the occurrence of paleocurrents to the southeast in the Araripe Basin.

The rift stage is recorded in the Afro-Brazilian depression by the development of an unconformity overlying the first sedimentary sequence (SEQ-1) and by the deposition of two sedimentary sequences (SEQ-2 and SEQ-3) (Kuchle et al., 2011), which correspond to the deposition of the Abaiara Formation in the Araripe Basin (Assine, 2007; Kuchle et al., 2011). In the Araripe Basin, the rift stage is marked by the increase of Tonian zircon grains (Table 3, Fig. 6) and the contribution of the Central Sub-province eastern terranes (Fig. 10). Additionally, the significant percentage of Cariris Velhos ages (0.9–1.0 Ga) (Table 3) suggests that the eastern terranes (Piancó-Alto Brigida and Alto Pajeú) constituted a topographic high during the rift climax suggesting a separation between the Araripe and Sergipe–Alagoas basins. Our findings are in agreement with the suggestions of Scherer et al. (2014), who proposed a regional rearrangement of the paleodrainage system at the end of the first rift stage deposition related to fragmentation tectonic activity between Africa and South America (Fig. 10).

In the early Aptian (120 Ma) the continental break-up occurred between the Brazilian northeast and the western African basins (Potiguar and Benin, Pernambuco–Paraíba and Rio Muni; Jequitinhonha–Camumu and Gabon basins) (Heine et al., 2013). At ca. 115 Ma, the South Atlantic and Equatorial rift systems broke up and started experiencing post-rift thermal subsidence (Milani et al., 2007; Heine et al., 2013). In the Araripe Basin, the Aptian post-rift I successions were deposited. The basal Barbalha Formation correlates with the Marizal Formation in the Recôncavo–Tucano–Jatobá Basin and presents similar fluvial paleoflow (N–NW to S–SE) (Assine, 1994, 2007; Freitas et al., 2017). The Batateiras layer (Assine, 2007) is deposited in a lake under anoxic conditions and correlates with the Trairi Layer (Ceará Basin) and Ponta do Tubarão Layer (Potiguar Basin) (Hashimoto et al., 1987; Assine, 2007). Our data suggest a change in the source areas compared to the rift phase with contributions from N–NW to S–SE sources, similar to what is observed in the rift-beginning stage. This interpretation is based on the decrease in Tonian U–Pb zircon ages, and the increase in Paleoproterozoic and Neoproterozoic zircon ages (Fig. 5, Table 3). Our data further suggest that the eastern region stops to supply detritus to the Araripe Basin. Furthermore, our findings suggest that the area located to the E–NE of the Araripe Basin, which was a source during the rift stage, was not a topographic high during the Aptian.

The Albian–Cenomanian post-rift II fluvial and alluvial Araripina and Exu formations are characterized by paleocurrent directions toward WSW (Assine, 1994; Godot Souza et al., 2022, and this study; see Supplementary Fig. S1) with probably proximal eastern sources. We ascribed this change in provenance to the Albian–Cenomanian uplift of the Borborema plateau that occurred after the Gondwana breakup (Assine, 2007; Eagles, 2007; Eagles and König, 2008; Matos et al., 2021a, 2021b), as indicated by the increases of Archean and Neoproterozoic zircons in the sedimentary rocks of the Exu Formation. This uplift may have induced drainage reorganization at the local scale such as in the Araripe Basin (this study), Potiguar Basin (Baesso et al., 2021), and São Luís–Grajaú Basin (Nascimento et al., 2007), and also at the regional scale such as in Guyana (Roddaz et al., 2021; Girault et al., 2023). This drainage reorganization along the Equatorial margin was also contemporaneous with the establishment of the so-called "Sanozama" paleodrainage in western Amazonia (Rodrigues et al., 2023), which might suggest that the entire northern part of South America experienced major drainage reorganization in response to the post-rift uplift of the equatorial Atlantic rifting.

6. Conclusion

The provenance study of the sedimentary rocks of the Araripe Basin (NE Brazil) based on a multi-proxy dataset (major and trace element concentrations, Sm–Nd isotopic composition, and detrital zircon U–Pb ages) yields the following conclusions:

- The εNd (0) values (−12.3 to −23.7) together with the T_{DM} ages (1.68 to 2.55 Ga) suggest an old crustal source for the sedimentary rocks analyzed. The presence of Rhyacian to Orosirian (2.3–1.8 Ga) and Ediacaran (0.63–0.54 Ga) U–Pb zircon ages further suggests the dominant contribution of the Borborema Province basement, influenced by the Brasiliano cycle (650–520 Ma).
- The low contribution of Tonian (~940 Ma) grains to the U–Pb zircon age distribution, with published paleocurrent direction, suggests sources located in the northern and northwestern terranes of the Borborema Province, probably near the Parnaíba lineament (Patos shear zone), the rift-beginning stage;
- The increase of Stenian–Tonian (1.2–0.72 Ga) zircon grains in the U–Pb zircon age distribution of the Abaiara Formation suggests a dominant source located in the eastern terranes during the rift stage.
- The significant percentage of Cariris Velhos ages (0.9–1.0 Ga) further indicates that the eastern terranes (Riacho do Gravatá and Alto Pajeú) constituted a topographic high during the rift climax, which may have separated the Araripe and Sergipe–Alagoas basins;
- The decrease of Tonian U–Pb zircon ages and the increase of Paleoproterozoic and Neoproterozoic zircon ages in the U–Pb zircon age distributions of the post-rift I sedimentary rocks (Santana Group) suggest a change in the source areas with sources located in the northern terranes of the Borborema Province similar to what is observed in the rift beginning stage;
- The Albian–Cenomanian post-rift II fluvial and alluvial Araripina and Exu formations are characterized by dominant contributions of Paleoproterozoic and Cryogenian–Ediacaran (720–541 Ma) zircon ages, which we interpret to suggest proximal sources located in the NE. We ascribed this change in provenance to the Albian to Cenomanian uplift of the Borborema plateau during the Equatorial Atlantic Ocean formation.

Finally, similarly to other recently published studies, our provenance data emphasize the major role played by the post-rift uplift of the Brazilian craton in shaping the late Cretaceous paleodrainage of the northern part of South America.

Supplementary data to this article can be found online at https://doi.org/10.1016/j.sedgeo.2024.106680.

CRediT authorship contribution statement

Mariana de Assunção Rodrigues: Writing – review & editing, Writing – original draft, Visualization, Validation, Methodology, Investigation, Formal analysis, Data curation, Conceptualization. **Roberto Ventura Santos:** Writing – review & editing, Visualization, Validation, Supervision, Project administration, Methodology, Investigation, Funding acquisition, Data curation, Conceptualization. **Martin Roddaz:** Writing – review & editing, Visualization, Validation, Supervision, Methodology, Investigation, Funding acquisition, Data curation, Conceptualization. **Elton Luiz Dantas:** Writing – review & editing, Visualization, Validation. **Mathieu Leisen:** Writing – review & editing, Visualization, Validation, Methodology, Data curation.

Data availability

All geochemical and geochronological data, as well as the compiled database, major and trace element uncertainties, and correlation coefficients, are uploaded into an online supplementary dataset associated with this paper (Rodrigues, Mariana; Santos, Roberto; Roddaz, Martin; Dantas, Elton Luiz; Leisen, Mathieu (2024), "U–Pb ages and zircon composition of the Araripe Basin Rodrigues et al. in Revision", Mendeley Data, V3, doi: 10.17632/mzwnxgz8zb.2) in Mendley Data Repository.

Declaration of competing interest

The authors declare that they have no known competing financial interests or personal relationships that could have appeared to influence the work reported in this paper.

Acknowledgments

We are thankful to the University of Brasilia and University Toulouse III Paul Sabatier for the infrastructure and technical support. We also thank for the financial support of the Brazilian National Council for Scientific and Technological Development (CNPq-428843/2916-6; 312941/2018-8), the Coordination for the Improvement of Higher Education Personnel – Brazil (CAPES) Finance Code 001, and the French Evaluation Committee of the University and Scientific Cooperation with Brazil (COFECUB) for funding the first author during the Ph.D. degree. This study was also supported and financed by CAPES-COFECUB program Te 924/18 "Paléo-Amazone: évolution Néogène de l'Amazonie Brésilienne." This paper is based on the academic thesis written by the first author during the Ph.D. degree. We thank two anonymous reviewers and the editor Catherine Chagué for valuable reviews that improved this contribution.

References

Albarède, F., Brouxel, M., 1987. The Sm/Nd secular evolution of the continental crust and the depleted mantle. Earth and Planetary Science Letters 82, 25–35. https://doi.org/10.1016/0012-821X(87)90104-X.

Almeida, F.F.M., Hasui, Y., de Brito Neves, B.B., Fuck, R.A., 1981. Brazilian structural provinces: an introduction. Earth-Science Reviews 17, 1–29. https://doi.org/10.1016/0012-8252(81)90003-9.

Amaral, W.S., Kraus, R.K., Dantas, E.L., Fuck, R.A., Pitombeira, J.P.A., 2017. Sinistral reactivation of the Transbrasiliano Lineament: structural and geochronological evidences in the Cariré Granulite Zone, Borborema Province - NE Brazil. Journal of South American Earth Sciences 79, 409–420. https://doi.org/10.1016/j.jsames.2017.08.022.

Angelim, L.A.A., Kosin, M., 2001. Estados da Bahia, Pernambuco e Piaui: Escala 1:500.000, Programa Levantamentos Geológicos Básicos do Brasil - PLGB. CPRM-Serviço Geológico do Brasil, Rio de Janeiro (in Portuguese).

Arai, M., 2014. Aptian/Albian (Early Cretaceous) paleogeography of the South Atlantic: a paleontological perspective. Brazilian Journal of Geology 44, 339–350. https://doi.org/10.5327/Z2317-4889201400020012.

Arai, M., 2016. Reply to the comments of Assine et al. (Comments on paper by M. Arai "Aptian/Albian (Early Cretaceous) paleogeography of the South Atlantic: a paleontological perspective"). Brazilian Journal of Geology 46, 9–13. https://doi.org/10.1590/2317-4889201620150046B.

Araujo, C.E.G., Cordani, U.G., Basei, M.A.S., Castro, N.A., Sato, K., Sproesser, W.M., 2012. U–Pb detrital zircon provenance of metasedimentary rocks from the Ceará Central and Médio Coreaú Domains, Borborema Province, NE-Brazil: tectonic implications for a long-lived Neoproterozoic active continental margin. Precambrian Research 206-207, 36–51. https://doi.org/10.1016/j.precamres.2012.02.021.

Archanjo, C.J., de Hollanda, M.H.B.M., Viegas, L.G.F., 2021. Late Ediacaran lateral-escape tectonics as recorded by the Patos shear zone (Borborema Province, NE Brazil). Brazilian Journal of Geology 51, e20200132. https://doi.org/10.1590/2317-4889202120200132.

Arthaud, M.H., Caby, R., Fuck, R.A., Dantas, E.L., Parente, C.V., 2008. Geology pf the northern Borborema Province, NE Brazil and its correlation with Nigeria, NW Africa. Geological Society of London, Special Publication 294, 49–67. https://doi.org/10.1144/SP294.4.

Arthaud, M.H., Fuck, R.A., Dantas, E.L., Santos, T.J.S., Caby, R., Armstrong, R., 2015. The Neoproterozoic Ceará Group, Ceará Central domain, NE Brazil: depositional age and provenance of detrital material. New insights from U–Pb and Sm–Nd geochronology. Journal of South American Earth Sciences 58, 223–237. https://doi.org/10.1016/j.jsames.2014.09.007.

Assine, M.L., 1992. Analise estratigrafica da Bacia do Araripe, Nordeste do Brasil. RBG 22, 289–300 (in Portuguese) 10.25249/0375-7536.1992289300.

Assine, M.L., 1994. Paleocorrentes e Paleogeografia na Bacia do Araripe, Nordeste do Brasil. Revista Brasileira de Geociencias 24, 223–232 (in Portuguese) 10.25249/0375-7536.1994223232.

Assine, M.L., 2007. Bacia do Araripe. Boletim de Geociências da Petrobras 15, 371–389 (in Portuguese).

Assine, M.L., Neumann, H., Varejão, F.G., Mescolotti, P.C., 2014. Sequências deposicionais do Andar Alagoas da Bacia do Araripe, Nordeste do Brasil. Boletim de Geociências da Petrobras 22, 3–28 (in Portuguese).

Assis, A.P., Porto, A.L., Schmitt, R.S., Linol, B., Medeiros, S.R., Correa Martins, F., Silva, D.S., 2019. The Ordovician–Silurian tectono-stratigraphic evolution and paleogeography of eastern Parnaiba Basin, NE Brazil. Journal of South American Earth Sciences 95, 102241. https://doi.org/10.1016/j.jsames.2019.102241.

Augustsson, C., Bahlburg, H., 2008. Provenance of late Palaeozoic metasediments of the Patagonian proto-Pacific margin (southernmost Chile and Argentina). International Journal of Earth Sciences (Geol Rundsch) 97, 71–88. https://doi.org/10.1007/s00531-006-0158-7.

Augustsson, C., Voigt, T., Bernhart, K., Kreißler, M., Gaupp, R., Gärtner, A., Hofmann, M., Linnemann, U., 2018. Zircon size-age sorting and source-area effect: the German Triassic Buntsandstein Group. Sedimentary Geology 375, 218–231. https://doi.org/10.1016/j.sedgeo.2017.11.004.

Baesso, A., Remus, M.V.D., Pereira, B.R.B., Alkmim, A.R., Lana, C.C., Vignol-Lelarge, M.L., Porcher, C.C., 2021. Insights into sedimentary provenance and the evolution of the Potiguar Basin, NE Brazil, using U–Pb ages and Lu–Hf isotopes in detrital zircons. Marine and Petroleum Geology 131, 105170. https://doi.org/10.1016/j.marpetgeo.2021.105170.

Barbosa, J.A., Hessel, M.H., Nascimento, M.C. do, Neumann, V.H., 2006. Ocorrência de Taenidium Barreti na Formação Rio da Batateira, Crétacéo da Bacia do Araripe. Estudos Geológicos 16, 50–60 (in Portuguese).

Basu, A.R., Sharma, M., DeCelles, P.G., 1990. Nd, Sr-isotopic provenance and trace element geochemistry of Amazonian foreland basin fluvial sands, Bolivia and Peru: implications for ensialic Andean orogeny. Earth and Planetary Science Letters 100, 1–17. https://doi.org/10.1016/0012-821X(90)90172-T.

Beaudoin, A., 2003. A comparation of two methods for estimating the organic content of sediments. Journal of Paleolimnology 29, 387–390. https://doi.org/10.1023/B:JOPL.0000042999.30131.5b.

Beurlen, K., 1962. A geologia da Chapada do Araripe. Anais da Academia Brasileira de Ciências 34, 365–370 (in Portuguese).

Bleeker, W., 2003. The late Archean record: a puzzle in ca. 35 pieces. Lithos 71, 99–134. https://doi.org/10.1016/j.lithos.2003.07.003.

Bock, B., Mclennan, Hanson, 1998. Geochemistry and provenance of the Middle Ordovician Austin Glen Member (Normanskill Formation) and the Taconian Orogeny in New England. Sedimentology 45, 635–655. https://doi.org/10.1046/j.1365-3091.1998.00168.x.

Bom, M.H.H., Ceolin, D., Kochhann, K.G.D., Krahl, G., Fauth, G., Bergue, C.T., Savian, J.F., Strohschoen Junior, O., Simões, M.G., Assine, M.L., 2021. Paleoenvironmental evolution of the Aptian Romualdo Formation, Araripe Basin, Northeastern Brazil. Global and Planetary Change 203, 103528. https://doi.org/10.1016/j.gloplacha.2021.103528.

Bouchez, J., Gaillardet, J., France-Lanord, C., Maurice, L., Dutra-Maia, P., 2011. Grain size control of river suspended sediment geochemistry: clues from Amazon River depth profiles: river sediments grain size and chemistry. Geochemistry, Geophysics, Geosystems 12. https://doi.org/10.1029/2010GC003380.

Brito, L.M., 1987. As unidades litoestratigraficas da passagem Jurassico-Cretaceo do Nordeste do Brasil. Revista Brasileira de Geociencias 17, 81–85 (in Portuguese).

Brito Neves, B.B., Santos, T.J.S.S., Dantas, E.L., 2022. O Terreno Tectonoestratigrafico São Pedro: Oeste da Zona TRansversal - Provincia Borborema. Geologia USP, Série Científica 22, 45–69 (in Portuguese with English abstract) https://doi.org/10.11606/issn.2316-9095.v22-197489.

Brune, S., Kolawole, F., Olive, J.-A., Stamps, D.S., Tech, V., Buck, W.R., Buiter, S.J.H., 2023. Geodynamics of continental rift initiation and evolution. Nature Reviews Earth and Environment 4, 235–253.

Camacho, C.R., Sousa, F.R.F.R. de O., 2017. O arcabouço estrutural da Bacia Sedimentar do Araripe, Província Borborema, baseado em dados aeromagnetométricos. Geologia USP. Série Científicavol. 17, p. 149. https://doi.org/10.11606/issn.2316-9095.v17-393 (in Portuguese).

Caputo, M.V., Crowell, J.C., 1985. Migration of glacial centers across Gondwana during Paleozoic Era. Geological Society of America Bulletin 96, 1020–1036. https://doi.org/10.1130/0016-7606(1985)96<1020:MOGCAG>2.0.CO;2.

Carignan, J., Hild, P., Mevelle, G., Morel, J., Yeghicheyan, D., 2001. Routine analyses of trace elements in geological samples using flow injection and low pressure on-line liquid chromatography coupled to ICP-MS: a study of geochemical reference materials BR,

DR-N, UB-N, AN-G and GH. Geostandards and Geoanalytical Research 25, 187–198. https://doi.org/10.1111/j.1751-908X.2001.tb00595.x.
Caxito, F.A., Uhlein, A., Dantas, E., Stevenson, R., Egydio-Silva, M., Salgado, S.S., 2017. The Rio Preto and Riacho do Pontal Belts. In: Heilbron, M., Cordani, U.G., Alkmim, F.F. (Eds.), São Francisco Craton, Eastern Brazil. Regional Geology Reviews. Springer International Publishing, Cham, pp. 221–239 https://doi.org/10.1007/978-3-319-01715-0_12.
Caxito, F.D.A., Santos, L.C.M.D.L., Ganade, C.E., Bendaoud, A., Fettous, E.-H., Bouyo, M.H., 2020. Toward an integrated model of geological evolution for NE Brazil-NW Africa: the Borborema Province and its connections to the Trans-Saharan (Benino-Nigerian and Tuareg shields) and Central African orogens. Brazilian Journal of Geology 50, e20190122. https://doi.org/10.1590/2317-4889202020190122.
Cerri, R.I., Warren, L.V., Spencer, C.J., Varejão, F.G., Promenzio, P., Luvizotto, G.L., Assine, M.L., 2022. Using detrital zircon and rutile to constrain sedimentary provenance of Early Paleozoic fluvial systems of the Araripe Basin, Western Gondwana. Journal of South American Earth Sciences 116, 103821. https://doi.org/10.1016/j.jsames.2022.103821.
Coimbra, J.C., Arai, M., Carreño, A.L., 2002. Biostratigraphy of Lower Cretaceous microfossils from the Araripe basin, northeastern Brazil. Geobios 35, 687–698.
Condie, K.C., 1993. Chemical composition and evolution of the upper continental crust: contrasting results from surface samples and shales. Chemical Geology 104, 1–37. https://doi.org/10.1016/0009-2541(93)90140-E.
Costa, F.G. da, Araújo, C.E.G. de, Amaral, W. da S., Vasconcelos, A.M., Rodrigues, J.B., 2013. U–Pb (LA-ICPMS) zircon ages and Nd isotopes for granitoids of the Tamboril-Santa Quitéria Complex, Ceará Central Domain: implication for neoproterozoic syncollisional magmatism in north Borborema Province. Geologia USP. Série Científica vol. 13, pp. 159–174. https://doi.org/10.5327/Z1519-874X2013000200009.
Cullers, R.L., 2000. The geochemistry of shales, siltstones and sandstones of Pennsylvanian–Permian age, Colorado, USA: implications for provenance and metamorphic studies. Lithos 51, 181–203. https://doi.org/10.1016/S0024-4937(99)00063-8.
Custódio, M.A., Quaglio, F., Warren, L.V., Simões, M.G., Fürsich, F.T., Perinotto, J.A.J., Assine, M.L., 2017. The transgressive–regressive cycle of the Romualdo Formation (Araripe Basin): sedimentary archive of the Early Cretaceous marine ingression in the interior of Northeast Brazil. Sedimentary Geology 359, 1–15. https://doi.org/10.1016/j.sedgeo.2017.07.010.
da Cruz, R.F., Pimentel, M.M., Accioly, A.C. de A., Rodrigues, J.B., 2014. Geological and isotopic characteristics of granites from the Western Pernambuco–Alagoas Domain: implications for the crustal evolution of the Neoproterozoic Borborema Province. Brazilian Journal of Geology 44, 627–652. https://doi.org/10.5327/Z2317488920140004008.
Dantas, E.L., Van Schumus, W.R., Hackespacher, P.C., Fetter, A.H., Brito Neves, B.B., Cordani, U., Nutman, A.P., Williams, I.S., 2004. The 3.4-3.5 Ga São João do Campestre massif, NE Brazil: remnants of the oldest crust in South America. Precambrian Research 130, 113–137. https://doi.org/10.1016/j.precamres.2003.11.002.
Dantas, E.L., Souza, Z.S., Wenrnick, E., Hackspacher, P.C., Martin, H., Xiaodong, D., Li, J.W., 2013. Crustal growth in the 3.4-2.7 Ga São José de Campestre Massif, Borborema Province, NE Brazil. Precambrian Research 227, 120–156. https://doi.org/10.1016/j.precamres.2012.08.006.
De Baar, H.J.W., Bacon, M.P., Brewer, P.G., Bruland, K.W., 1985. Rare earth elements in the Pacific and Atlantic Oceans. Geochimica et Cosmochimica Acta 49, 1943–1959. https://doi.org/10.1016/0016-7037(85)90089-4.
de Brito Neves, B.B., Campos Neto, M.D.C., 2016. A faixa de dobramentos do Rio Salgado, norte-noroeste da Zona Transversal-Província Borborema (PB-CE). Geolologia USP. Série científica vol. 16, p. 3. https://doi.org/10.11606/issn.2316-9095.v16i3p3-17 (in Portuguese).
de Brito Neves, B.B., Passarelli, C.R., 2020. Terrenos tectonoestratigráficos dispersos do embasamento pré-Brasiliano (São José do Caiana, Açude Coremas e Icaiçara) na porção centro-oeste da Zona Transversal (Paraíba, Ceará e Pernambuco). Geolologia USP. Série Científica vol. 20, pp. 81–105. https://doi.org/10.11606/issn.2316-9095.v20-159425 (in Portuguese).
de Brito Neves, B.B., Santos, E.J.D., Van Schmus, W.R., 2000. Tectonic history of the Borborema Province, Northeast Brazil. Tectonic Evolution of South America. 31st International Geological Congress, Rio de Janeiro, pp. 151–182.
de Brito Neves, B.B., Neto, M.C.C., Van Schmus, W.R., Fernandes, M.G., Souza, S.L., 2001. O Terreno Alto Moxoto no leste da Paraiba ("Maciço Caldas Brandão"). Revista Brasileira de Geociencias 31, 135–194 (in Portuguese with English abstract).
de Brito Neves, B.B., Passarelli, C.R., Basei, M.A.S., dos Santos, E.J., 2003. Idades U-Pb em zircão de alguns granitos clássicos da Província Borborema. Geologia USP. Série Científica vol. 3, pp. 25–38. https://doi.org/10.5327/S1519-874X2003000100003 (in Portuguese).
de Brito Neves, B.B., Van Schmus, W.R., Kozuch, M., dos Santos, E.J., Petronilho, L., 2005. A Zona Tectônica Teixeira Terra Nova - ZTTTN - fundamentos da geologia regional e isotópica. Geologia USP. Série Científica vol. 5, pp. 57–80. https://doi.org/10.5327/S1519-874X2005000100005 (in Portuguese).
de Brito Neves, B.B., Van Schmus, W.R., Angelim, L.A.A., 2015. Contribuição ao conhecimento da evolução geológica do Sistema Riacho do Pontal – PE, BA, PI. Geologia USP, Série científica 15, 57–93 (in Portuguese with English abstract) https://doi.org/10.11606/issn.2316-9095.v15i1p57-93.
de Brito Neves, B.B., dos Santos, T.J.S., Dantas, E.L., 2023. O Terreno Tectonoestratigráfico São Pedro: Oeste da Zona Transversal – Província Borborema. Geologia USP. Série Científica vol. 22, pp. 45–69. https://doi.org/10.11606/issn.2316-9095.v22-197489 (in Portuguese).
De Castro, D.L., Fuck, R.A., Phillips, J.D., Vidotti, R.M., Bezerra, F.H.R., Dantas, E.L., 2014. Crustal structure beneath the Paleozoic Parnaíba Basin revealed by airborne gravity and magnetic data, Brazil. Tectonophysics 614, 128–145. https://doi.org/10.1016/j.tecto.2013.12.009.
D'el Rey Silva, L.J.H., 1995. The evolution of basement gneiss domes of the Sergipano fold belt (NE Brazil) and its importance for the analysis of Proterozoic basins. Journal of South American Earth Sciences 8, 325–340.
DePaolo, D.J., 1981. Trace element and isotopic effects of combined wallrock assimilation and fractional crystallization. Earth and Planetary Science Letters 53, 189–202. https://doi.org/10.1016/0012-821X(81)90153-9.
DePaolo, D.J., Linn, A.M., Schubert, G., 1991. The continental crustal age distribution: methods of determining mantle separation ages from Sm–Nd isotopic data and application to the southwestern United States. Journal of Geophysical Research 96, 2071. https://doi.org/10.1029/90JB02219.
Dummann, W., Hofmann, P., Herrle, J.O., Frank, M., Wagner, T., 2023. The early opening of the Equatorial Atlantic gateway and the evolution of Cretaceous peak warming. Geology 51, 476–480. https://doi.org/10.1130/G50842.1.
Eagles, G., 2007. New angles on South Atlantic opening. Geophysical Journal International 168, 353–361. https://doi.org/10.1111/j.1365-246X.2006.03206.x.
Eagles, G., König, M., 2008. A model of plate kinematics in Gondwana breakup. Geophysical Journal International 173, 703–717. https://doi.org/10.1111/j.1365-246X.2008.03753.x.
Ebert, H., 1970. The Precambrian geology of the Borborema Belt (states of Paraíba and Rio Grande do Norte, northeastern Brazil), and the origin of its mineral resources. Geologische Rundschau 59, 1294–1326.
Fambrini, G.L., Neumann, V.H. de M.L., Barros, C.L. de, Silva, S.M.O.A. da, Galm, P.C., de Menezes Filho, J.A.B., 2013. Análise estratigráfica da Formação Brejo Santo, Bacia do Araripe, Nordeste do Brasil: implicações paleogeográficas. Geologia USP. Série Científica vol. 13, pp. 3–28. https://doi.org/10.5327/Z1519-874X201300040001 (in Portuguese).
Fambrini, G.L., Menezes-Filho, J.A.B., Jesuíno, P.C.L., Silvestre, D.D.C., Neumann, V.H.M.L., de Lemos, D.R., 2016. Characterization of the depositional systems of the Barbalha formation, Araripe basin, northeastern Brazil. Comunicações Geológicas 103, 51–65.
Fambrini, G.L., Silva-Filho, W.F. da, Lemos, D.R. de, Silvestre, D.D.C., Araújo, J.T. de, Menezes-Filho, J.A.B. de, Tesser Junior, S., Neumann, V.H.D.M.L., 2019. Análise tectonossedimentar das fases início de rifte e clímax de rifte da Bacia do Araripe, Nordeste do Brasil. Geologia USP. Série Científica vol. 19, pp. 205–236. https://doi.org/10.11606/issn.2316-9095.v19-150526 (in Portuguese).
Fambrini, G.L., Silvestre, D. da C., Barreto Junior, A.M., Silva-Filho, W.F. da, 2020. Estratigrafia da Bacia do Araripe: estado da arte, revisão crítica e resultados novos. Geologia USP. Série Científicavol. 20, pp. 169–212. https://doi.org/10.11606/issn.2316-9095.v20-163467 (in Portuguese).
Fedo, C.M., Wayne Nesbitt, H., Young, G.M., 1995. Unraveling the effects of potassium metasomatism in sedimentary rocks and paleosols, with implications for paleoweathering conditions and provenance. Geology 23, 921. https://doi.org/10.1130/0091-7613(1995)023<0921:UTEOPM>2.3.CO;2.
Ferreira, V.P., Sial, A.N., Jardim de Sá, E.F., 1998. Geochemical and isotopic signatures of Proterozoic granitoids in terranes of the Borborema structural province, northeastern Brazil. Journal of South American Earth Sciences 11, 439–455. https://doi.org/10.1016/S0895-9811(98)00027-3.
Fetter, A.H., Schmus, W.R.V., Santos, T.J.S.D., Nogueira Neto, J.A., Arthaud, M.H., 2000. U–Pb And Sm–Nd geochronological constraints on the crustal evolution and basement architecture of Ceará State, Nw Borborema Province, Ne Brazil: implications for the existence of the paleoproterozoic supercontinent "Atlantica". Revista Brasileira de Geosciências 30, 102–106. https://doi.org/10.25249/0375-7536.2000301102106.
Figueiredo, J., Hoorn, C., Ven, P. van der, Soares, E., 2009. Late Miocene onset of the Amazon River and the Amazon deep-sea fan: evidence from the Foz do Amazonas Basin. Geology 37, 619–622. https://doi.org/10.1130/G25567A.1.
Freimann, M. de A., 2014. Geocronologia e petrotrama de quartzo milonitos do duplex transcorrente de Lavras da Mangabeira (Mestrado em Petrologia Ígnea e Metamórfica). Universidade de São Paulo, São Paulo https://doi.org/10.11606/D.44.2014.tde-26112014-144455 (in Portuguese with abstract in English).
Freitas, B.T., Almeida, R.P., Carrera, S.C., Figueiredo, F.T., Turra, B.B., Varejão, F.G., Assine, M.L., 2017. Aptian sedimentation in the Recôncavo–Tucano–Jatobá Rift System and its tectonic and paleogeographic significance. Journal of South American Earth Sciences 80, 460–481. https://doi.org/10.1016/j.jsames.2017.10.001.
Garcia, A.J.V., Wilbert, A., 1995. Paleogeographic evolution of Mesozoic pre-rift sequences in costal and interior basins of Northeastern Brazil. Pangea: Global Environments and Resources. Canadian Society of Petroleum Geologists, Calgary, pp. 123–130.
Gärtner, A., Linnemann, U., Sagawe, A., Hofmann, M., Ullrich, B., Kleber, A., 2013. Morphology of zircon crystal grains in sediments — characteristics, classifications, definitions// Morphologie von Zirkonen in Sedimenten – Merkmale, Klassifikationen, Definitionen. Jounal of Central European Geology 59, 65–73.
Girault, I., Basile, C., Bernet, M., Paquette, J., Heuret, A., Loncke, L., Poetisi, E., Balvay, M., 2023. Thermochronology and U–Pb dating of detrital zircons from the Demerara Plateau (French Guiana-Suriname): implications for the provenance of the Early Cretaceous syn-rift sedimentation. Basin Research 35, 1386–1406. https://doi.org/10.1111/bre.12758.
Godot Souza, J.F., Isozaki, Y., Tsutsumi, Y., Schmitt, R. da S., Medeiros, S.R. de, Almeida, C.N. de, Araujo, B.C., Richetti, P., da Silva, E.A., Rios Netto, A. de M., 2022. Provenance analysis of the Araripe intracontinental basin, northeast Brazil — routes for proto-Atlantic marine incursions in northwest Gondwana. Sedimentary Geology 440, 106243. https://doi.org/10.1016/j.sedgeo.2022.106243.
Góes, A.M., 1995. A Formação Poti (Carbonifero Inferior) da Bacia do Parnaíba (Tese de doutoramento). Universidade de São Paulo, São Paulo (in Portuguese with abstract in English).
Góes, A.M., Feijó, F.J., 1994. Bacia do Parnaíba. Boletim de Geociências da Petrobras 8, 57–67 (in Portuguese).
Goia, S.M.C.L., Pimentel, M.M., 2000. The Sm–Nd isotopic method in the geochronology laboratory of the University of Brasília. Anais da Academia Brasileira de Ciências 72, 219–245. https://doi.org/10.1590/S0001-37652000000200009.
Goldstein, S.L., O'Nions, R.K., Hamilton, P.J., 1984. A Sm–Nd isotopic study of atmospheric dusts and particulates from major river systems. Earth and Planetary Science Letters 70, 221–236. https://doi.org/10.1016/0012-821X(84)90007-4.

Guimarães, I.P., de Fatima, L., de Brito, M., Lages, G. de A., da Silva Filho, A.F., Santos, L., Brasilino, R.G., 2016. Tonian granitic magmatism of the Borborema Province, NE Brazil: a review. Journal of South American Earth Sciences 68, 97–112. https://doi.org/10.1016/j.jsames.2015.10.009.

Guzmán-González, J., Sial, A.N., Piovesan, E.K., Oliveira, E.V., Fambrini, G.L., 2020. Paleolimnological reconstruction of a marginal area of Jurassic Capianga Lake, Jatobá Basin, northeast Brazilian. Journal of Paleolimnology 63, 113–128. https://doi.org/10.1007/s10933-019-00105-0.

Hall, S.A., Bird, D.E., McLean, D.J., Towle, P.J., Grant, J.V., Danque, H.A., 2018. New constraints on the age of the opening of the South Atlantic basin. Marine and Petroleum Geology 95, 50–66. https://doi.org/10.1016/j.marpetgeo.2018.03.010.

Hashimoto, A.T., Appi, C.J., Soldan, A.L., Cerqueira, J.R., 1987. O Neo-Alagoas nas Bacias do Ceara, Araripe e Potiguar (Brasil): Caracterização estratigrafica e Paleoambiental. Revista Brasileira de Geosciências 17, 118–122. https://doi.org/10.25249/0375-7536.1987118122.

Heilbron, M., Guedes, E., Mane, M., Valeriano, C. de M., Tupinambá, M., Almeida, J., Silva, L.G. do E., Paschoal Duarte, B., Favera, J.C.D., Viana, A., 2018. Geochemical and temporal provinciality of the magmatism of the eastern Parnaíba Basin, NE Brazil. Geological Society, London, Special Publications 472, 251–278. https://doi.org/10.1144/SP472.11.

Heimhofer, U., Hochuli, P.-A., 2010. Early Cretaceous angiosperm pollen from a low-latitude succession (Araripe Basin, NE Brazil). Review of Palaeobotany and Palynology 161, 105–126. https://doi.org/10.1016/j.revpalbo.2010.03.010.

Heine, C., Zoethout, J., Müller, R.D., 2013. Kinematics of the South Atlantic rift. Solid Earth 4, 215–253. https://doi.org/10.5194/se-4-215-2013.

Heiri, O., Lotter, A.F., Lemcke, G., 2001. Loss on ignition as a method for estimating organic and carbonate content in sediments: reproducibility and comparability of results. Journal of Paleolimnology 25, 101–110. https://doi.org/10.1023/A:1008119611481.

Hollanda, M.H.B.M., Archanjo, C.J., Souza, L.C., Dunyi, L., Armstrong, R., 2011. Long-lived Paleoproterozoic granitic magmatism in the Seridó–Jaguaribe domain, Borborema Province—NE Brazil. Journal of South American Earth Sciences 32, 287–300. https://doi.org/10.1016/j.jsames.2011.02.008.

Hollanda, M.H.B.M., Goes, A.M., Silva, D.B., Negri, F.A., 2014. Proveniência sedimentar dos arenitos da Bacia do Parnaíba (NE do Brasil). Boletim de Geociências da Petrobras 22, 191–211 (in Portuguese).

Hollanda, M.H.B.M., Góes, A.M., Negri, F.A., 2018. Provenance of sandstones in the Parnaíba Basin through detrital zircon geochronology. Geological Society, London, Special Publications 472, 181–197. https://doi.org/10.1144/SP472.16.

Hoorn, C., Bogotá-A, G.R., Romero-Baez, M., Lammertsma, E.I., Flantua, S.G.A., Dantas, E.L., Dino, R., do Carmo, D.A., Chemale, F., 2017. The Amazon at sea: onset and stages of the Amazon River from a marine record, with special reference to Neogene plant turnover in the drainage basin. Global and Planetary Change 153, 51–65. https://doi.org/10.1016/j.gloplacha.2017.02.005.

Horbe, A.M.C., Roddaz, M., Gomes, L.B., Castro, R.T., Dantas, E.L., Do Carmo, D.A., 2019. Provenance of the neogene sediments from the Solimoes formation (Solimoes and Acre basins), Brazil. Journal of South American Earth Sciences 93, 232–241.

Huck, C.E., Van de Flierdt, T., Jiménez-Espejo, F.J., Bohaty, S.M., Röhl, U., Hammond, S.J., 2016. Robustness of fossil fish teeth for seawater neodymium isotope reconstructions under variable redox conditions in an ancient shallow marine setting. Geochemistry, Geophysics, Geosystems 17, 679–698. https://doi.org/10.1002/2015GC006218.

Jackson, S.E., Pearson, N.J., Griffin, W.L., Belousova, E.A., 2004. The application of laser ablation-inductively coupled plasma-mass spectrometry to in situ U–Pb zircon geochronology. Chemical Geology 211, 47–69. https://doi.org/10.1016/j.chemgeo.2004.06.017.

Jacobsen, S.B., Wasserburg, G.J., 1980. Sm–Nd isotopic evolution of chondrites. Earth and Planetary Science Letters 50, 139–155. https://doi.org/10.1016/0012-821X(80)90125-9.

Jardim Sá, E.F., Macedo, M.H.E., Fuck, R.A., Kawashita, K., 1992. Terrenos Proterozoicos na Provincia Borborema e a Margem Norte do Craton São Francisco. Revista Brasileira de Geosciências 22, 742–780. https://doi.org/10.25249/0375-7536.1991472480.

Jochum, K.P., Weis, U., Stoll, B., Kuzmin, D., Yang, Q., Raczek, I., Jacob, D.E., Stracke, A., Birbaum, K., Frick, D.A., Günther, D., Enzweiler, J., 2011. Determination of reference values for NIST SRM 610-617 glasses following ISO guidelines. Geostandards and Geoanalytical Research 35, 397–429. https://doi.org/10.1111/j.1751-908X.2011.00120.x.

Kennedy, A.K., Wotzlaw, J.-F., Schaltegger, U., Crowley, J.L., Schmitz, M., 2014. Eocene zircon reference material for microanalysis of U–Th–Pb isotopes and trace elements. Canadian Mineralogist 52, 409–421. https://doi.org/10.3749/canmin.52.3.409.

Klöcking, M., White, N., MacLennan, J., 2018. Role of basaltic magmatism within the Parnaíba cratonic basin, NE Brazil. Geological Society, London, Special Publications 472, 309–319. https://doi.org/10.1144/SP472.4.

Kozuch, M., 2003. Isotopic and Trace Elements Geochemistry of Early Neoproterozoic Gneissic and Metavolcanic Rocks in the CaririsVelhos Orogen of the Borborema Province, Brazil, and Their Bearing on Tectonic Setting. University of Kansas, Lawrence (PhD Thesis).

Kuchle, J., Scherer, C.M. dos S., Born, C.C., Alvarenga, R. dos S., Adegas, F., 2011. A contribution to regional stratigraphic correlations of the Afro-Brazilian depression — the Dom João Stage (Brotas Group and equivalent units — Late Jurassic) in Northeastern Brazilian sedimentary basins. Journal of South American Earth Sciences 31, 358–371. https://doi.org/10.1016/j.jsames.2011.02.007.

Lages, G.A., de Lira, Montefalco, Santos, L.C., Brasilino, R.G., Rodrigues, J.B., Dantas, E.L., 2019. Statherian–Calymmian (ca. 1.6 Ga) magmatism in the Alto Moxotó Terrane, Borborema Province, northeast Brazil: implications for within-plate and coeval collisional tectonics in West Gondwana. Journal of South American Earth Sciences 91, 116–130. https://doi.org/10.1016/j.jsames.2019.02.003.

Lima, M.R. de, 1978. Palinologia da Formação Santana (Cretaceo do Nordeste do Brasil). Univesidade de São Paulo, São Paulo (PhD Thesis, in Portuguese with abstract in English).

Lima, M.R. de, Perinotto, J.A.J., 1984. Palinologia de sedimentos da parte superior da Formação Missão Velha, Bacia do Araripe. Geociências 3, 67–76 (in Portuguese).

Machado Junior, D. de L., Dehira, L.K., Carneiro, C. dal R., Almeida, F.F.M. de, 1990. Reconstruções Paleoambientais do Juro-Cretaceo no Nordeste Oriental Brasileiro. Revista Brasileira de Geociencias 19, 470–485 (in Portuguese with abstract in English).

MacRae, N.D., Nesbitt, H.W., Kronberg, B.I., 1992. Development of a positive Eu anomaly during diagenesis. Earth and Planetary Science Letters 109, 585–591. https://doi.org/10.1016/0012-821X(92)90116-D.

Maisey, J.G., 2000. Continental break up and the distribution of fishes of Western Gondwana during the Early Cretaceous. Cretaceous Research 21, 281–314. https://doi.org/10.1006/cres.1999.0195.

Marsh, J.H., Jørgensen, T.R.C., Petrus, J.A., Hamilton, M.A., Mole, D.R., 2019. U–Pb, trace element, and hafnium isotope composition of the Maniitsoq zircon: a potential new Archean zircon reference material. Abstracts. Presented at the Goldschmidt, Geochemical Society, Barcelona.

Martin, E.E., Scher, H.D., 2004. Preservation of seawater Sr and Nd isotopes in fossil fish teeth: bad news and good news. Earth and Planetary Science Letters 220 (1–2), 25–39. https://doi.org/10.1016/S0012-821X(04)00030-5.

Matos, R.M.D., 1992. The Northeast Brazilian Rift System. Tectonics 11, 766–791. https://doi.org/10.1029/91TC03092.

Matos, R.M.D. de, 1999. History of the northeast Brazilian rift system: kinematic implications for the break-up between Brazil and West Africa. SP 153, 55–73. https://doi.org/10.1144/GSL.SP.1999.153.01.04.

Matos, R.M.D. de, Krueger, A., Norton, I., Casey, K., 2021a. The fundamental role of the Borborema and Benin–Nigeria provinces of NE Brazil and NW Africa during the development of the South Atlantic Cretaceous Rift system. Marine and Petroleum Geology 127, 104872. https://doi.org/10.1016/j.marpetgeo.2020.104872.

Matos, R.M.D. de, Medeiros, W.E., Jardim de Sá, E.F., Almeida, C.B. de, Norton, I., Córdoba, V.C., 2021b. A solution to the Albian fit challenge between the South American and African plates based on key magmatic and sedimentary events late in the rifting phase in the Pernambuco and Paraíba basins. Marine and Petroleum Geology 128, 105038. https://doi.org/10.1016/j.marpetgeo.2021.105038.

McLennan, S.M., Taylor, S.R., McCulloch, M.T., Maynard, J.B., 1990. Geochemical and Nd Sr isotopic composition of deep-sea turbidites: crustal evolution and plate tectonic associations. Geochimica et Cosmochimica Acta 54, 2015–2050. https://doi.org/10.1016/0016-7037(90)90269-Q.

McLennan, S.M., Hemming, S., McDaniel, D.K., Hanson, G.N., 1993. Geochemical approaches to sedimentation, provenance and tectonics. Processes Controlling the Composition of Clastic Sediments. Geological Society of America, Colorado.

Milani, E.J., Rangel, H.D., Bueno, G.V., Stica, J.M., Winter, W.R., Caixeta, J.M., Neto, O. da C.P., 2007. Bacias Sedimentares Brasileiras - Cartas Estratigraficas. Boletim de Geociências da Petrobras 15, 183–205 (in Portuguese).

Miloski, P., Mendes, J.C., Almeida, C.N. de, de Castro Valente, S., Regina de Medeiros, S., 2019. Petrogenesis of continental flood basalts in eastern Parnaiba basin, Brazil: a singular sill occurrence with low- and high-TiO2 tholeiites. Journal of South American Earth Sciences 94, 102192. https://doi.org/10.1016/j.jsames.2019.05.008.

Moiroud, M., Pucéat, E., Donnadieu, Y., Bayon, G., Guiraud, M., Voigt, S., Deconinck, J.-F., Monna, F., 2016. Evolution of neodymium isotopic signature of seawater during the Late Cretaceous: implications for intermediate and deep circulation. Gondwana Research 36, 503–522. https://doi.org/10.1016/j.gr.2015.08.005.

Moulin, M., Aslanian, D., Unternehr, P., 2010. A new starting point for the South and Equatorial Atlantic Ocean. Earth-Science Reviews 98, 1–37. https://doi.org/10.1016/j.earscirev.2009.08.001.

Nascimento, M.D.S., Góes, A.M., Macambira, M.J.B., Brod, J.A., 2007. Provenance of Albian sandstones in the São Luís–Grajaú Basin (northern Brazil) from evidence of Pb–Pb zircon ages, mineral chemistry of tourmaline and palaeocurrent data. Sedimentary Geology 201, 21–42. https://doi.org/10.1016/j.sedgeo.2007.04.005.

Nesbitt, H.W., Young, G.M., 1982. Early Proterozoic climates and plate motions inferred from major element chemistry of lutites. Nature 299.

Neumann, V.H., Borrego, A.G., Cabrera, L., Dino, R., 2003. Organic matter composition and distribution through the Aptian–Albian lacustrine sequences of the Araripe Basin, northeastern Brazil. International Journal of Coal Geology 54, 21–40. https://doi.org/10.1016/S0166-5162(03)00018-1.

Neves, S.P., 2003. Proterozoic history of the Borborema province (NE Brazil): Correlations with neighboring cratons and Pan-African belts and implications for the evolution of western Gondwana. Tectonics 22, 1031. https://doi.org/10.1029/2001TC001352.

Neves, S.P., Lages, G.A., Brasilino, R.G., Miranda, A.W.A., 2015. Paleoproterozoic accretionary and collisional processes and the build-up of the Borborema Province (NE Brazil): geochronological and geochemical evidence from the Central Domain. Journal of South American Earth Sciences 58, 165–187. https://doi.org/10.1016/j.jsames.2014.06.009.

Parente, C.V., Arthaud, M.H., 1995. O Sistema Orós-Jaguaribe no Ceará, NE do Brasil. Revista Brasileira de Geosciências 25, 297–306. https://doi.org/10.25249/0375-7536.1995297306 (in Portuguese with abstract in English).

Paton, C., Hellstrom, J., Paul, B., Woodhead, J., Hergt, J., 2011. Iolite: freeware for the visualisation and processing of mass spectrometric data. Journal of Analytical Atomic Spectrometry 26, 2508. https://doi.org/10.1039/c1ja10172b.

Petrus, J.A., Kamber, B.S., 2012. VizualAge: a novel approach to laser ablation ICP-MS U–Pb geochronology data reduction. Geostandards and Geoanalytical Research 36, 247–270. https://doi.org/10.1111/j.1751-908X.2012.00158.x.

Pimentel, M.M., Fuck, R.A., 1992. Neoproterozoic crustal accretion in central Brazil. Geology 20, 375. https://doi.org/10.1130/0091-7613(1992)020<0375:NCAICB>2.3.CO;2.

Ponte, F.C., Appi, C.J., 1990. Proposta de revisão da coluna litoestratigrafica da Bacia do Araripe. Anais. Presented at the Congresso Brasileiro de Geologia, Sociedade Brasileira de Geologia, Natal, pp. 211–226 (in Portuguese).

Ponte, F.C., Ponte Filho, F.C., 1996. Estrutura geológica e evolução tectônica da Bacia do Araripe. DNPM, Recife (in Portuguese).
Pourmand, A., Dauphas, N., Ireland, T.J., 2012. A novel extraction chromatography and MC-ICP-MS technique for rapid analysis of REE, Sc and Y: revising CI-chondrite and Post-Archean Australian Shale (PAAS) abundances. Chemical Geology 291, 38–54. https://doi.org/10.1016/j.chemgeo.2011.08.011.
Powers, M.C., 1953. A new roundness scale for sedimentary particles. Journal of Sedimentary Petrology 23, 117–119. https://doi.org/10.1306/D4269567-2B26-11D7-8648000102C1865D.
Prado, L.A.C.D., Pereira, P.A., Sales, A.M.F., Barreto, A.M.F., 2015. Taphonomic and paleoenvironmental considerations for the concentrations of macroinvertibrate fossils in the Romualdo Member, Santana Formation, Late Aptian–Early Albian, Araripe Basin, Araripina, NE, Brazil. Journal of South American Earth Sciences 62, 218–228. https://doi.org/10.1016/j.jsames.2015.06.005.
Rios Netto, A. de M., Paula-Freitas, A.B.L., Carvalho, I. de S., Regali, M. da S.P., Borghi, L., Freitas, F.I. de, 2012a. Formalização estratigráfica do Membro Fundão, Formação Rio da Batateira, Cretáceo Inferior da Bacia do Araripe, Nordeste do Brasil. Revista Brasileira de Geociencias 42. https://doi.org/10.5327/Z0375-75362012000200005 (in Portuguese with abstract in English).
Rios Netto, A. de M., Regali, M. da S.P., Carvalho, I. de S., Freitas, F.I. de, 2012b. Palinoestratigrafia do intervalo Alagoas da Bacia do Araripe, Nordeste do Brasil. Revista Brasileira de Geociencias 42. https://doi.org/10.5327/Z0375-75362012000200009 (in Portuguese with abstract in English).
Roddaz, M., Viers, J., Brusset, S., Baby, P., Hérail, G., 2005. Sediment provenances and drainage evolution of the Neogene Amazonian foreland basin. Earth and Planetary Science Letters 239, 57–78. https://doi.org/10.1016/j.epsl.2005.08.007.
Roddaz, M., Christophoul, F., Burgos Zambrano, J.D., Soula, J.-C., Baby, P., 2012. Provenance of late Oligocene to quaternary sediments of the Ecuadorian Amazonian foreland basin as inferred from major and trace element geochemistry and Nd–Sr isotopic composition. Journal of South American Earth Sciences 37, 136–153. https://doi.org/10.1016/j.jsames.2012.02.008.
Roddaz, M., Viers, J., Moreira-Turcq, P., Blondel, C., Sondag, F., Guyot, J.-L., Moreira, L., 2014. Evidence for the control of the geochemistry of Amazonian floodplain sediments by stratification of suspended sediments in the Amazon. Chemical Geology 387, 101–110. https://doi.org/10.1016/j.chemgeo.2014.07.022.
Roddaz, M., Dera, G., Mourlot, Y., Calvès, G., Kim, J.-H., Chaboureau, A.-C., Mounic, S., Raisson, F., 2021. Provenance constraints on the Cretaceous–Paleocene erosional history of the Guiana Shield as determined from the geochemistry of clay-size fraction of sediments from the Arapaima-1 well (Guyana–Suriname basin). Marine Geology 434, 106433.
Rodrigues, M. de A., 2023. Análise da proveniência de sedimentos das bacias cretáceas do sistema Andes-Amazônia-Margem Equatorial e sua relação com a paleogeografia e tectônica. Universidade de Brasília, Brasília (Tese de doutoramento, in Portuguese with abstract in English and French).
Rodrigues, S.W.O., de Brito Neves, B.B., 2008. Padrões isotópicos Sm-Nd no limite entre os terrenos Alto Pajeu e Alto Moxoto (PB). Revista Brasileira de Geociencias 38, 209–225 (in Portuguese with English abstract).
Rodrigues, M. de A., Roddaz, M., Santos, R.V., Louterbach, M., D'Apolito, C., Brusset, S., Dantas, E.L., Negri, F.R., 2023. New insights into the Cretaceous evolution of the Western Amazonian paleodrainage system. Sedimentary Geology 453, 106434. https://doi.org/10.1016/j.sedgeo.2023.106434.
Sahabi, M., Aslanian, D., Olivet, J.-L., 2004. Un nouveau point de départ pour l'histoire de l'Atlantique central. Comptes Rendus Geoscience 336, 1041–1052. https://doi.org/10.1016/j.crte.2004.03.017.
Sales, A.M.F., 2005. Análise tafonômica das ocorrências fossiliferas de macroinvertebrados do Membro Romualdo (Albiano) da Formação Santana, Bacia do Araripe, NE do Brasil: Significado estratigrafico e paleoambiental (Tese de doutoramento). Universidade de São Paulo, São Paulo (in Portuguese with abstract in English).
Santos, T.J.S. dos, Fetter, A.H., Neto, J.A., Hackspacher, P.C., Van Schmus, R., 1998. Geochronology and geochemistry of the Medio Coreau Domain NW Borborema Province. XL Congresso Brasileiro de Gologia.
Santos, E.J., Nutman, A.P., Brito Neves, B.B., 2004. Idades SHRIMP U-Pb do Complexo Sertânia: implicações sobre a evolução tectônica da Zona Transversal, Província Borborema. Revista do Instituto de Geociências – USP. Série Cientifica 4, 1–12 (in Portuguese with English abstract).
Santos, T.J.S., Fetter, A.H., Neto, J.A.N., 2008. Comparisons between the northwestern Borborema Province, NE Brazil, and the southwestern Pharusian Dahomey Belt, SW Central Africa. Geological Society, London, Special Publications 294, 101–120. https://doi.org/10.1144/SP294.6.
Santos, E.J., Schmus, W.R.V., Kozuch, M., Neves, B.B. de B., 2010. The Cariris Velhos tectonic event in Northeast Brazil. Journal of South American Earth Sciences 29, 61–76. https://doi.org/10.1016/j.jsames.2009.07.003.
Scherer, C.M. dos S., Jardim de Sá, E.F., Córdoba, V.C., Sousa, D. do C., Aquino, M.M., Canelas Cardoso, F.M., 2014. Tectono-stratigraphic evolution of the Upper Jurassic–Neocomian rift succession, Araripe Basin, Northeast Brazil. Journal of South American Earth Sciences 49, 106–122. https://doi.org/10.1016/j.jsames.2013.10.007.
Scherer, C.M.S., Goldberg, K., Bardola, T., 2015. Facies architecture and sequence stratigraphy of an early post-rift fluvial succession, Aptian Barbalha Formation, Araripe Basin, northeastern Brazil. Sedimentary Geology 322, 43–62. https://doi.org/10.1016/j.sedgeo.2015.03.010.
Shirey, S.B., Richardson, S.H., 2011. Start of the Wilson cycle at 3 Ga shown by diamonds from subcontinental mantle. Science 333, 434–436. https://doi.org/10.1126/science.1206275.
Silva Filho, M.A., Torres, H.H.F., 2002. A new interpretation on the Sergipano belt Domain. Anais da Academia Brasileira de Ciências 74, 556–557 (in Portuguese).
Silvestre, D., Fambrini, G., Santos, A., 2017. Caracterização Faciológica das Formações Cariri e Brejo Santo em Afloramentos a ne do Município Missão Velha (Ceará – Brasil). Estudos Geológicos 27, 19–33. https://doi.org/10.18190/1980-8208/estudosgeologicos.v27n1p19-33.
Sláma, J., Košler, J., Condon, D.J., Crowley, J.L., Gerdes, A., Hanchar, J.M., Horstwood, M.S.A., Morris, G.A., Nasdala, L., Norberg, N., Schaltegger, U., Schoene, B., Tubrett, M.N., Whitehouse, M.J., 2008. Plešovice zircon — a new natural reference material for U–Pb and Hf isotopic microanalysis. Chemical Geology 249, 1–35. https://doi.org/10.1016/j.chemgeo.2007.11.005.
Spencer, C.J., Kirkland, C.L., Taylor, R.J.M., 2016. Strategies towards statistically robust interpretations of in situ U–Pb zircon geochronology. Geoscience Frontiers 7, 581–589. https://doi.org/10.1016/j.gsf.2015.11.006.
Taylor, S.R., McClennan, S.M., 1985. The Continental Crust: Its Composition and Evolution: An Examination of the Geochemical Record Preserved in Sedimentary Rocks. Blackwell Scientific, Oxford.
Tribovillard, N.-P., Caulet, J.-P., Vergnaud-Grazzini, C., Moureau, N., Tremblay, P., 1996. Lack of organic matter accumulation on the upwelling-influenced Somalia margin in a glacial–interglacial transition. Marine Geology 133, 157–182. https://doi.org/10.1016/0025-3227(96)00034-5.
Van Kranendonk, M.J., Hugh Smithies, R., Hickman, A.H., Wingate, M.T.D., Bodorkos, S., 2010. Evidence for Mesoarchean (~3.2Ga) rifting of the Pilbara Craton: the missing link in an early Precambrian Wilson cycle. Precambrian Research 177, 145–161. https://doi.org/10.1016/j.precamres.2009.11.007.
Van Schmus, W.R., de Brito Neves, B.B., Williams, I.S., Hackspacher, P.C., Fetter, A.H., Dantas, E.L., Babinski, M., 2003. The Seridó Group of NE Brazil, a late Neoproterozoic pre- to syn-collisional basin in West Gondwana: insights from SHRIMP U–Pb detrital zircon ages and Sm–Nd crustal residence (TDM) ages. Precambrian Research 127, 287–327. https://doi.org/10.1016/S0301-9268(03)00197-9.
van Schmus, W.R., Oliveira, E.P., da Silva Filho, A.F., Toteu, S.F., Penaye, J., Guimarães, I.P., 2008. Proterozoic links between the Borborema Province, NE Brazil, and the Central African Fold Belt. Geological Society, London, Special Publications 294, 69–99. https://doi.org/10.1144/SP294.5.
Van Schmus, W.R., Kozuch, M., de Brito Neves, B.B., 2011. Precambrian history of the Zona Transversal of the Borborema Province, NE Brazil: insights from Sm–Nd and U–Pb geochronology. Journal of South American Earth Sciences 31, 227–252. https://doi.org/10.1016/j.jsames.2011.02.010.
Van Schumus, W.R., Kozuch, M., Brito Neves, B.B., 2011. Precambrian history of the Zona Transversal of the Borborema Province, NE Brazil: insights from Sm-Nd and U-Pb geochronology. Journal of South American Earth Sciences 31, 227–326.
van Soelen, E.E., Kim, J.-H., Santos, R.V., Dantas, E.L., Vasconcelos de Almeida, F., Pires, J.P., Roddaz, M., Sinninghe Damsté, J.S., 2017. A 30 Ma history of the Amazon River inferred from terrigenous sediments and organic matter on the Ceará Rise. Earth and Planetary Science Letters 474, 40–48. https://doi.org/10.1016/j.epsl.2017.06.025.
Vaz, P.T., Rezende, N. das G. de A., Wanderley Filho, J.R., Travassos, W.A.S., 2007. Bacia do Parnaíba. Boletim de Geociências da Petrobras. vol. 15, pp. 253–263 (in Portuguese with abstract in English).
Vermeesch, P., 2004. How many grains are needed for a provenance study? Earth and Planetary Science Letters 224, 441–451. https://doi.org/10.1016/j.epsl.2004.05.037.
Vermeesch, P., 2013. Multi-sample comparison of detrital age distributions. Chemical Geology 341, 140–146. https://doi.org/10.1016/j.chemgeo.2013.01.010.
Vermeesch, P., 2018. Dissimilarity measures in detrital geochronology. Earth-Science Reviews 178, 310–321. https://doi.org/10.1016/j.earscirev.2017.11.027.
Vieira, D.S.C., 2019. Geocronologia U-Pb e geiauimica isotopica Hf-Nd dos ortognaisses e granitoides da região de Granjeiro-Varzea Alegre (CE), Dominio Rio Grande do Norte (Dissertação de mestrado). Universidade Federal do Pará, Belém (in Portuguese with abstract in English).
Vieira Melo, B.G., Carvalho, I.S., 2018. The Brejo Santo Formation Fauna, Neojurassic from Araripe Basin, Brazil: paleoenvironmental interpretations. Anuário IGEO UFRJ 40, 62–74. https://doi.org/10.11137/2017_3_62_74.
Viers, J., Wasserburg, G.J., 2004. Behavior of Sm and Nd in a lateritic soil profile. Geochimica et Cosmochimica Acta 68, 2043–2054. https://doi.org/10.1016/j.gca.2003.10.034.
Weis, D., Kieffer, B., Maerschalk, C., Pretorius, W., Barling, J., 2005. High-precision Pb–Sr–Nd–Hf isotopic characterization of USGS BHVO-1 and BHVO-2 reference materials: Pb–Sr–Nd–Hf characterization. Geochemistry, Geophysics, Geosystems 6. https://doi.org/10.1029/2004GC000852.
Wiedenbeck, M., Allé, P., Corfu, F., Griffin, W.L., Meier, M., Oberli, F., Von Quadt, A., Roddick, J.C., Spiegel, W., 1995. Three natura zircon standards for U–Th–Pb, Lu–Hf, trace element and REE analyses. Geostandards Newsletter 19, 1–23.
Wiedenbeck, M., Hanchar, J.M., Peck, W.H., Sylvester, P., Valley, J., Whitehouse, M., Kronz, A., Morishita, Y., Nasdala, L., Fiebig, J., Franchi, I., Girard, J.-P., Greenwood, R.C., Hinton, R., Kita, N., Mason, P.R.D., Norman, M., Ogasawara, M., Piccoli, P.M., Rhede, D., Satoh, H., Schulz-Dobrick, B., Skår, O., Spicuzza, Mj, Terada, K., Tindle, A., Togashi, S., Vennemann, T., Xie, Q., Zheng, Y.-F., 2004. Further characterisation of the 91500 zircon crystal. Geostandards and Geoanalytical Research 28, 9–39. https://doi.org/10.1111/j.1751-908X.2004.tb01041.x.
Wilson, J.T., 1969. Static or mobile earth: the current scientific revolution. Tectonophysics 7, 600–601. https://doi.org/10.1016/0040-1951(69)90033-X.